ON PHYSICS OF INTERCALATION OF MOLECULAR HYDROGEN NANOPHASE INTO GRAPHENE SURFACE NANOBLISTERS, RELEVANCE FOR SOLVING THE HYDROGEN STORAGE PROBLEM

Yu S. Nechaev[1] and T. Nejat Veziroglu[2]

[1]Bardin Institute for Ferrous Metallurgy, Kurdjumov Institute of Metals Science and Physics, Vtoraya Baumanskaya St., 9/23, Moscow 105005, Russia.
[2]International Association for Hydrogen Energy, 5794 SW 40 St. #303, Miami, FL 33155, USA.

1. Introduction

As it is noted in a number of articles of 2007 through 2014, hydrogenation of graphene-layers-systems, as a prototype of covalent chemical functionality and an effective tool to open the band gap of graphene, has both fundamental and applied importance [1, 2].

It is related to the current problems of thermodynamic stability and thermodynamic characteristics of the hydrogenated graphene-layers-systems [3–19]; those are related to the very current problem of hydrogen on-board efficient storage in fuel-cell-powered vehicles [14–19].

The latter problem has been studied by many scientists in different developed countries, in the framework of the state and private large grant projects, for the recent not less than 25 years, but it has not been solved up to nowadays.

In the present paper, our modified results [14–19] of thermodynamic analysis of a number of theoretical and experimental data on "reversible" hydrogenation and dehydrogenation of some graphene-layer-nanostructures are considered. The physics of intercalation of molecular hydrogen nanophase of a high density into carbon-based nanostructures is also considered. It is relevant for developing of a key breakthrough nanotechnology of the hydrogen on-board efficient and compact storage in fuel-cell-powered vehicles, i.e. for solving the above noted current problem.

Constructive critical discussions on the present and [14–18] results, and/or the International cooperation seem as a real way of a joint breakthrough solving of the hydrogen efficient storage problem. To attract attention and/or to involve a number of the related scientists to such a way is one of the main aims of our recent publications, including the aim of overcoming some psychological barrier obviously existing for many scientists due to their numerous unsuccessful attempts in solving this problem.

As it is above noted, the present analytical study is related to a further development and modification of our previous analytical results, particularly published in the **open access** journals [16, 17]. Therefore, the related figures (Figs.) from [16, 17] are referred in the present paper.

2. Consideration of some energetic characteristics of theoretical [3, 20] graphanes

In work [3], the stability of graphane, a fully saturated extended two-dimentional hydrocarbon derived from a single graphene sheet with formula CH, has been predicted on the basis of the first principles and total-energy calculations. All of the carbon atoms are in sp^3 hybridization forming a hexagonal network (a strongly diamond-like distorted graphene network) and the hydrogen atoms are bonded to carbon on both sides of the plane in an alternative manner. It has been found that graphane can have two favorable conformations: a chair-like (diamond-like, Fig. 1 in [16]) conformer and a boat-like (zigzag-like) conformer [3].
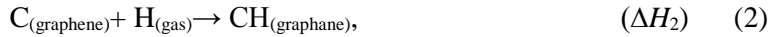
The diamond-like conformer (Fig. 1 in [16]) is more stable than the zigzag-like one. This was concluded from the results of the calculations [3] of the two quantities: 1) binding energy $\Delta H_{\text{bind.(graphane[3])}}$ − the difference between the total energy of the isolated atoms and the total energy of the compounds; 2) the standard energy of formation $\Delta H^0_{\text{f298(graphane[3])}}$ of the compounds ($CH_{\text{(graphane[3])}}$) from crystalline graphite ($C_{\text{(graphite)}}$) and gaseous molecular hydrogen ($H_{2\text{(gas)}}$) at the standard pressure and temperature conditions.

For the diamond-like graphane, the former quantity is $\Delta H_{\text{bind.(graphane[3])}} = 6.56$ eV/atom, and the latter one is $\Delta H_{1[3]} = \Delta H^0_{f\,298(graphane[3])} = -0.15$ eV/atom. The $\Delta H_{1[3]}$ quantity corresponds to the following reaction:

$$C_{(graphite)} + \tfrac{1}{2}H_{2(gas)} \rightarrow CH_{(graphane)}, \qquad (\Delta H_1) \qquad (1)$$
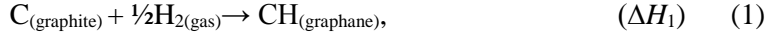
where ΔH_1 is the standard energy (enthalpy) change for this reaction.

By using the theoretical quantity of $\Box H^0_{f\,298(graphane[3])}$, one can evaluate, using the framework of the thermodynamic method of cyclic processes [21], a value of the energy of formation $\Delta H_{2[3]})$ of graphane $CH_{(graphane[3])}$ from graphene $C_{(graphene)}$ and gaseous atomic hydrogen $H_{(gas)}$. For this, it is necessary to take into consideration the following three additional reactions:

$$C_{(graphene)} + H_{(gas)} \rightarrow CH_{(graphane)}, \qquad (\Delta H_2) \qquad (2)$$

$$C_{(graphene)} \rightarrow C_{(graphite)}, \qquad (\Delta H_3) \qquad (3)$$

$$H_{(gas)} \rightarrow \tfrac{1}{2}\,H_{2(gas)}, \qquad (H_4) \qquad (4)$$

where ΔH_2, ΔH_3 and ΔH_4 are the standard energy (enthalpy) changes.

Reaction (2) can be presented as a sum of reactions (1), (3) and (4) using the framework of the thermodynamic method of cyclic processes [21]:

$$\Delta H_2 = (\Delta H_3 + \Delta H_4 + \Delta H_1). \qquad (5)$$

Substituting in Eq. (5) the known experimental value [22] of $\Delta H_{4[22]} = -2.26$ eV/atom , the value of $\Delta H_{3[20,22]} \Box -0.05$ eV/atom, and the theoretical value [3] of $\Delta H_{1[3]} = -0.15$ эB/atom, one can obtain a desired value of $\Delta H_{2[3]} = -2.5 \pm 0.1$ eV/atom. The quantity of $-\Delta H_{2[3]}$ characterizes the break-down energy of C-H sp^3 bond in graphane [3] (Fig. 1 in [16]), relevant to the breaking away of one hydrogen atom from the material, which is $\Delta H_{(C\text{-}H)graphane[3]} = -\Delta H_{2[3]} = 2.5 \pm 0.1$ eV (Table 1A).

It is important to note that in our evaluating of the $\Delta H_{(C\text{-}H)graphane[3]}$ quantity, by the use of the method of cyclic processes [21] (Eqs. 1–5), only one ($\Delta H_{1[3]}=$ $\Box H^0_{f\,298(graphane[3])}$) from the two theoretical quantities ($\Box H^0_{f\,298(graphane[3])}$ and $\Delta H_{bind.(graphane[3])}$) has been used.

In evaluating the above mentioned value of ΔH_3, one can use the experimental data [22] on the graphite sublimation energy at 298 K ($\Delta H_{\text{subl.(graphite)[22]}}$ = 7.41 $\square$ 0.05 eV/atom), and the theoretical data [20] on the binding cohesive energy at about 0 K for graphene ($\Delta H_{\text{cohes.(graphene[20])}}$ = 7.40 eV/atom). Therefore, neglecting the temperature dependence of these quantities in the range of 0 to 298 K, one can obtain the above used value of $\Delta H_{3[20,22]}$ $\square$ –0.05 eV/atom.

The $\Delta H_{\text{cohes.(graphene)[20]}}$ quantity characterizes the break-down energy of 1.5 C-C sp^2 bond in graphene, relevant to the breaking away of one carbon atom from the material. Consequently, one can evaluate the break-down energy of C-C sp^2 bonds in graphene, which is $\Delta H_{\text{(C-C)graphene[20]}}$ = 4.93 eV. This theoretical value of the quantity $\Delta H_{\text{(C-C)graphene[20]}}$ coincides with the empirical value of the similar quantity obtained in [16], from $\Delta H_{\text{subl.(graphite)[22]}}$, for C-C sp^2 bonds in graphite ($\Delta H_{\text{(C-C)graphite[16,22]}}$ = 4.94 $\square$ 0.03 eV).

The empirical value of the similar quantity for C-C sp^3 bonds in diamond obtained in [16], from the diamond sublimation energy $\Delta H_{\text{subl.(diamond)[22]}}$, is $\Delta H_{\text{(C-C)diamond[16,22]}}$ = 3.69 $\square$ 0.02 eV.

By using both the $\Delta H_{\text{(C-H)graphane[3]}}$ quantity, and the $\Delta H_{\text{bind.(graphane[3])}}$ quantity, one can evaluate, in the framework of the method of cyclic processes [21], a value of the break-down energy of C-C sp^3 bonds in the theoretical graphane [3], namely: $\Delta H_{\text{(C-C)graphane[3]}} \approx 2.7$ eV (Table 1A).

On the other hand, by using the $\Delta H_{\text{(C-H)graphane[3]}}$ quantity only, i.e. without using $\Delta H_{\text{bind.(graphane[3])}}$ quantity, one can evaluate, in the same framework of [21], a rather higher value of the break-down energy of C-C sp^3 bonds in the theoretical graphane [3], namely: $\Delta H_{\text{(C-C)*graphane[3]}} \approx 3.9$ eV that is close to the similar quantity for graphene (Table 1A).

This discrepancy between the $\Delta H_{\text{(C-C)graphane[3]}}$ and $\Delta H_{\text{(C-C)*graphane[3]}}$ values seems as an open question.

It is important to note that chemisorption of hydrogen on graphene was studied in [20], using atomistic simulations, with a second generation reactive empirical bond order of Brenner inter-atomic potential. As it has been shown, the cohesive energy of graphane CH in the ground state is $\Delta H_{\text{cohes.(graphane[20])}}$ = 5.03 eV/atom(C). This results in the binding energy of hydrogen, which is $\Delta H_{\text{(C-H)graphane[20]}}$ = 1.50 eV/atom(H) (Table 1A).

By using the above noted theoretical values of $\Delta H_{cohes.(graphane[20])}$ and $\Delta H_{(C-H)graphane[20]}$, one can evaluate, in the framework of the method of cyclic processes [21], the break-down energy of C-C sp^3 bonds as: $\Delta H_{(C-C)graphane[20]} = 2.35$ eV (Table 1A).

On the other hand, by using the $\Delta H_{(C-H)graphane[20]}$ quantity only, i.e. without using the $\Delta H_{bind.(graphane[20])}$ quantity, one can evaluate, in the same framework of [21], a much higher value of the break-down energy of C-C sp^3 bonds in the theoretical graphane [20], namely: $\Delta H_{(C-C)*graphane[20]} \approx 3.9$ eV that is close to the similar quantity for graphene.

This large discrepancy between the $\Delta H_{(C-C)graphane[20]}$ and $\Delta H_{(C-C)*graphane[20]}$ values also seems as an open question.

Table 1A

Theoretical, experimental and analytical quantities related to Items 1-4

Material	Value/Quantity				
	$\Delta H_{(C-H)}$, eV	$\Delta H_{(bind.)}$, eV	$\Delta H_{(C-C)}$, eV	$\Delta H_{(des.)}$, eV $\{\Delta H_{(ads.)}$, eV$\}$	$K_{0(des.)}$, s^{-1} $\{L \approx (D_{0app.}/K_{0(des.)})^{1/2}\}$
Graphane (CH) [3] (theory)	2.5±0.1 (analysis)	6.56 (theory)	2.7 (analysis)		
Graphane (CH) [20] (theory)	1.50 (theory)	5.03 (theory)	2.35 (analysis)		
Graphane (CH) [4] (theory)	2.46 ± 0.17 (analysis)			2.46 ± 0.17 (theory)	2.0·10^{15} (analysis)
Free-standing graphane-like membrane [5]. (experiment)	There are no experimental values in [5]			if 2.5 ± 0.1 if 2.6 ± 0.1 $\{1.0 ± 0.2\}$ (analysis)	then 7·10^{12} then 5·10^{13} ($K_{0(ads.)} \approx K_{0(des.)}$)
Hydrogenated epitaxial graphene [5] (experiment)	There are no experimental values in [5]			then 1.84 then 1.94 if 0.3 if 0.6 if 0.9 $\{0.3 ± 0.2\}$ (analysis)	if 7·10^{12} if 5·10^{13} then 0.2 then 80 then 3.5·10^4 ($K_{0(ads.)} \approx K_{0(des.)}$) $\{L \sqsubset d_{sample}\}$
Hydrogenated epitaxial* graphene [5], TDS-peak #1 (experiment)				0.6 ± 0.3 (as processes $\sqsubset$ I-II [14], $\sqsubset$ model "G") (analysis)	2·10^7 (or 2·10^3- 2·10^{11}) $\{L \sqsubset d_{sample}\}$ (analysis)

Material				$\Delta H_{(des.)}$, eV	$K_{0(des.)}$, s^{-1}
Hydrogenated epitaxial* graphene [5], TDS-peak #2 (experiment)				0.6 ± 0.3 (as for processes □ I-II [14], □ model "G") (analysis)	$1 \cdot 10^6$ (or $4 \cdot 10^2$-$2 \cdot 10^9$) $\{L \square d_{sample}\}$ (analysis)
Hydrogenated epitaxial* graphene [5], TDS-peak #3 (experiment)				0.23 ± 0.05 (as process □ I [14], □ models "F", "G") (analysis)	2.4 (or 0.8-7) $\{L \square d_{sample}\}$ (analysis)
Rigidly fixed hydrogenated graphene membrane [5] (experiment)	There are no experimental values in [5]			There are no experimental values in [5]	There are no experimental values in [5]
Graphene [20] (theory)		7.40 (theory)	4.93 (analysis)		
Graphite [22, 16] (empirical)		7.41 ± 0.05 (analysis)	4.94 ± 0.03 (analysis)		
Diamond [22, 16] (empirical)		7.38 ± 0.04 (analysis)	3.69 ± 0.02 (analysis)		

Table 1B

Theoretical, experimental and analytical quantities related to Items 1-11

Material	Value/Quantity				
	$\Delta H_{(C-H)}$, eV		$\Delta H_{(C-C)}$, eV	$\Delta H_{(des.)}$, eV	$K_{0(des.)}$, s^{-1}
Hydrofullerene $C_{60}H_{36}$ [13]	2.64 ± 0.01 (experiment)				
Hydrogenated carbon nanotubes (C_2H) [12]	2.5 ± 0.2 (theory)				
Hydrogenated isotropic graphite, graphite nano-fibers and nano-structured graphite [14] (experiment)	2.50 ± 0.03 (analysis, process III [14], model "F*")		4.94 ± 0.03 (analysis)	2.6 ± 0.03 (analysis, process III [14])	There are empirical values in [14] (analysis of experiment)
Hydrogenated isotropic graphite, graphite nano-fibers, nanostructured graphite, defected carbon nanotubes [14]	2.90 ± 0.05 (analysis, process II [14], models "H", "G" (Fig. 4 in [16]))			1.24 ± 0.03 (analysis, process II [14])	There are empirical values in [14] (analysis of experiment)
Hydrogenated isotropic graphite, carbon nanotubes [14] (experiment)	2.40 ± 0.05 (analysis, process I [14], models "F", "G" (Fig. 4) in [16])			0.21 ± 0.02 (analysis, process I [14])	There are empirical values in [14] (analysis of experiment)

Hydrogenated isotropic and pyrolytic and nanostructured graphite [14] (experiment)	3.77 ± 0.05 (analysis, process IV [14], models "C", "D" (Fig. 4) in [16])			3.8 ± 0.5 (analysis, process IV [14])	There are empirical values in [14] (analysis of experiment)

3. Consideration and interpretation of the data [4] on dehydrogenation of theoretical graphane, comparing with the related experimental data [5]

In [4], the process of hydrogen thermal desorption from graphane has been studied using the method of molecular dynamics. The temperature dependence (for $T =$ 1300–3000 K) of the time

($t_{0.01}$) of hydrogen desorption onset (i.e., the time $t_{0.01}$ of removal ~1% of the initial hydrogen concentration $C_0 \approx 0.5$ (in atomic fractions), $-\Delta C/C_0 \approx 0.01$, $C/C_0 \approx 0.99$) from the $C_{54}H_{7(54+18)}$ clustered with 18 hydrogen passivating atoms at the edges to saturate the dangling bonds of sp^3-hybridized carbon atoms have been calculated. The corresponding activation energy of $\Delta H_{(des.)} = E_a = 2.46 \pm 0.17$ eV and the corresponding (temperature independent) frequency factor A = $(2.1 \pm 0.5)\cdot10^{17}$ s^{-1} have also been calculated. The process of hydrogen desorption at $T =$ 1300–3000 K has been described in terms of the Arrhenius-type relationship

$$1/t_{0.01} = A \exp(-E_a / k_B T), \tag{6}$$

where k_B is the Boltzmann constant.

The authors [4] predicted that their results would not contradict the experimental data [5], according to which the nearly complete desorption of hydrogen ($-\Delta C/C_0 \approx$ 0.9, $C/C_0 \approx 0.1$) from a free-standing graphane membrane (Fig. 2B in [16]) was achieved by annealing it in argon at $T = 723$ K for 24 hours (i.e., $t_{0.9(membr.[5])723K} =$ $8.6\cdot10^4$ s). But, as the below presented analysis shows, this declaration [4] is not enough adequate.

By using Eq. (6), the authors [4] evaluated the quantity of $t_{0.01(graphane[4])}$ for $T = 300$ K (~$1\cdot10^{24}$ s) and for $T = 600$ K (~$2\cdot10^3$ s). However, they noted that the above two values of $t_{0.01(graphane)}$ should be considered as rough estimates. Indeed, using Eq. (6), one can evaluate the value of $t_{0.01(graphane[4])723K} \approx 0.7$ s for $T = 723$ K, which is much less (by five orders) than the $t_{0.9(membr.[5])723K}$ value in [5].

In the framework of the formal kinetics approximation of the first order rate reaction [21], a characteristic quantity for the reaction of hydrogen desorption is $\tau_{0.63}$ – the time of the removal of ~ 63 % of the initial hydrogen concentration C_0 (i.e., $-\Delta C/C_0 \approx 0.63$, $C/C_0 \approx 0.37$) from the hydrogenated graphene. Such a first order rate reaction (desorption) can be described by the following equations [14, 16, 21]:

$$d\,C\,/\,d\,t = -K\,C, \tag{7}$$

$$(C\,/\,C_0) = \exp(-K\,t) = \exp(-t\,/\,\tau_{0.63}), \tag{8}$$

$$K = (1/\tau_{0.63}) = K_0 \exp(-\Delta H_{des.}\,/\,k_B\,T), \tag{9}$$

where C is the averaged concentration at the annealing time t, $K = (1/\tau_{0.63})$ is the reaction (desorption) rate constant, $\Delta H_{des.}$ is the reaction (desorption) activation energy, and K_0 is the per-exponential (or frequency) factor of the reaction rate constant.

In the case of a diffusion rate limiting kinetics, the quantity of K_0 is related to a solution of the corresponding diffusion problem ($K_0 \approx D_0/L^2$, where D_0 is the per-exponential factor of the diffusion coefficient, L being the characteristic diffusion length) [14, 16].

In the case of a non-diffusion rate limiting kinetics, which is obviously related to the situation of [4, 5], the quantity of K_0 may be the corresponding vibration (for (C-H) bonds) frequency ($K_0 = \nu_{(C-H)}$), the quantity $\Delta H_{(des.)} = \Delta H_{(C-H)}$ (Table 1), and Eq. (9) is correspond to the Polanyi-Wigner one [14, 16].

By substituting in Eq. (8) the quantities of $t = t_{0.01(graphane[4])723K}$ and $(C/C_0) = 0.99$, one can evaluate the desired quantity $\tau_{0.63(graphane[4])723K} \approx 70$ s. Analogically, the quantity of $t_{0.9(graphane[4])723K} \approx 160$ s can be evaluated, which is less (by about three orders) than the experimental value [5] of $t_{0.9(membr.[5])723K}$. In the same manner, one can evaluate the desired quantity $\tau_{0.63(membr.[5])723K} \approx 3.8 \cdot 10^4$ s, which is higher (by about three orders) than $\tau_{0.63(graphane[4])723K}$.

By using Eq. (9) and supposing that $\Delta H_{des.} = E_a$ and $K = 1/\tau_{0.63(graphane[4])723K}$, one can evaluate the analytical quantity of $K_{0(graphane[4])} = 2 \cdot 10^{15}$ s^{-1} for graphane [4] (Table 1A).

By substituting in Eq. (9) the quantity of $K = K_{(membr.[5])723K} = 1/\tau_{0.63(membr.[5])723K}$ and supposing that $\Delta H_{des.(membr.[5])} \approx \Delta H_{C-H(graphane[3,4])} \approx 2.5$ eV [3, 16, 4] (Table 1A), one can evaluate the quantity of $K_{0(membr.[5])} = \nu_{(membr.[5])} \approx 7 \cdot 10^{12}$ s^{-1} for the experimental graphane membranes [5]. The obtained quantity of $\nu_{(membr.[5])}$ is less by one and a half orders of the vibrational frequency $\nu_{RD} = 2.5 \cdot 10^{14}$ s^{-1} corresponding to the D Raman peak (1342 cm^{-1}) for hydrogenated graphene membrane and epitaxial graphene on SiO$_2$ (Fig. 2 in [16]). The authors [5] attribute the activation of the D Raman peak in the hydrogenated samples to breaking of the translation symmetry of C-C sp^2 bonds after formation of C-H sp^3 bonds.

The quantity $\nu_{(membr.[5])}$ is less by one order of the value [23] of the vibration frequency $\nu_{HREELS} = 8.7 \cdot 10^{13}$ s^{-1} corresponding to an additional HREELS peak arising from C-H sp^3 hybridization; a stretching appears at 369 meV after a partial hydrogenation of the epitaxial graphene. The authors [23] suppose that this peak can be assigned to the vertical C-H bonding, giving direct evidence for hydrogen attachment on the epitaxial graphene surface.

Taking into account ν_{RD} and ν_{HREELS} quantities, and substituting in Eq. (9) quantities of $K = 1/\tau_{0.63(membr.[5])723K}$ and $K_0 \approx K_{0(membr.[5])} \approx \nu_{HREELS}$, one can evaluate $\Delta H_{des.(membr.[5])} = \Delta H_{C-H(membr.[5])} \approx 2.66$ eV (Table 1A). In such approximation, the obtained value of $\Delta H_{C-H(membr.[5])}$ coincides (within the errors) with the experimental value [13] of the break-down energy of C-H bonds in hydrofullerene C$_{60}$H$_{36}$ ($\Delta H_{C-H(C60H36)} = 2.64 \pm 0.01$ eV, Table 1B).

The above analysis of the related data shows that the thermodesorption characteristics of $\Delta H_{des.(membr.[5])} = \Delta H_{C-H(membr.[5])} = 2.6 \pm 0.1$ eV and $K_{0(membr.[5])} = \nu_{C-H(membr.[5])} \approx 5 \cdot 10^{13}$ s^{-1} (Table 1A) can be used for the experimental graphene membranes. The analysis also shows that this is a case for a non-diffusion rate limiting kinetics, when Eq. (9) corresponds to the Polanyi-Wigner one [14, 16]. Certainly, these tentative results could be directly confirmed and/or modified by receiving and treating within Eqs. (8, 9) of the experimental data on $\tau_{0.63}$ at several annealing temperatures.

The above noted fact that the empirical [5, 16] quantity $\tau_{0.63(membr.[5])723K}$ is much larger (by about 3 orders) than the theoretical [4, 16] one ($\tau_{0.63(graphane[4])723K}$), is consistent with that mentioned in [5]. The alternative possibility has been supposed in [5] that (i) the experimental graphane membrane (a free-standing one) may have "a more complex hydrogen bonding, than the suggested by the theory", and that (ii) graphane (CH) [3] may be "the until-now-theoretical material".

4. Consideration of the experimental data [5] on hydrogenation-dehydrogenation of mono- and bi-layer epitaxial graphenes, comparing with the related data [5] for free-standing graphene membranes

4.1. Characteristics of hydrogenation-dehydrogenation of mono-layer epitaxial graphenes

In [5], both the graphene membrane samples considered above, and the epitaxial graphene and bi-graphene samples on substrate SiO_2 were exposed to a cold hydrogen dc plasma for 2 hours to reach the saturation in the measured characteristics. They used a low-pressure (0.1 mbar) hydrogen-argon mixture of 10% H_2. Raman spectra for hydrogenated and subsequently annealed free-standing graphene membranes (Fig. 2**B** in [16]) are rather similar to those for epitaxial graphene samples (Fig. 2**A** in [16]), but with some notable differences.

If the samples hydrogenated simultaneously for 1 hour, and before reaching the saturation (a partial hydrogenation), the D peak area for a free-standing membrane was two factors greater than the area for graphene on a substrate (Fig. 2 in [16], the left inset), which indicates the formation of twice as many C-H sp^3 bonds in the membrane. This result also agrees with the general expectation that atomic hydrogen attaches to both sides of the membranes. Moreover, the D peak area became up to about three times greater than the G peak area after prolonged exposures (for 2 hours, a near-complete hydrogenation) of the membranes to atomic hydrogen.

The integrated intensity area of the D peak in Fig. 2**B** in [16] corresponding to the adsorbed hydrogen saturation concentration in the graphene membranes is larger by a factor of about 3 for the area of the D peak in Fig. 2**A** in [16], corresponding to the hydrogen concentration in the epitaxial graphene samples.

The above noted Raman spectroscopy data [5] on dependence of the concentration (C) of adsorbed hydrogen from the hydrogenation time (t) (obviously, at about 300 K) can be described with the equation [14, 21]:

$$(C_0 - C) / C_0 = \exp(-K t) = \exp(-t / \tau_{0.63}), \qquad (8^*)$$

where C_0 is the saturation value.

By using the above noted Raman spectroscopy data [5] (Fig. 2 in [16]), one can suppose that the near-saturation ((C/C_0) $\approx$ 0.95) time ($t_{0.95}$) for the free standing graphene membranes (at ~300 K) is about 3 h, and a maximum possible (but not defined experimentally) value of $C_{0(membr.)} \approx 0.5$ (atomic fraction, i.e. the atomic ratio (H/C) =1). Hence, using Eq. (8*) results in the quantities of $\tau_{0.63(membr.[5])hydr.300K} \approx 1.0$ h, $C_{3h(membr.[5])} \approx 0.475$, $C_{2h(membr.[5])} \approx 0.43$ and $C_{1h(membr.[5])} \approx 0.32$, where $C_{3h(membr.[5])}$, $C_{2h(membr.[5])}$ and $C_{1h(membr.[5])}$ being the adsorbed hydrogen concentration at the hydrogenation time (t) equal to 3 h, 2 h and 1 h respectively. It is expedient to note that the quantity of $C_{0(membr.[5])} \approx 0.5$ corresponds to the local concentration of $C_{0(membr.[5]one\_side)} \approx 0.33$ for each of the two sides of a membrane, i.e. the local atomic ratio (H/C) = 0.50.

The obtained value of $\tau_{0.63(membr.[5])hydr.300K}$ (for process of hydrogenation of the free standing graphene membranes [5]) is much less (by about 26 orders) of the evaluated value of the similar quantity of $\tau_{0.63(membr.[5])dehydr.300K} \approx (0.4 - 2.7) \cdot 10^{26}$ h (if $\Delta H_{(des.)} = (2.49 - 2.61)$ eV, $K_{0(des.)} = (0.7 - 5) \cdot 10^{13}$ s^{-1}, Item 3, Table 1A) for process of dehydrogenation of the same free standing graphene membranes [5]. It shows that the activation energy of the hydrogen adsorption ($\Delta H_{(ads.)}$) for the free standing graphene membranes [5] is considerably less, than the activation energy of the hydrogen desorption ($\Delta H_{(des.)} = (2.5$ or $2.6)$ eV). Hence, by using Eq. 9 and supposing that $K_{0(ads.)} \approx K_{0(des.)}$, one can obtain a reasonable value of $\Delta H_{(ads.)membr.[5]} = 1.0 \pm 0.2$ eV (Table 1). The heat of adsorption of atomic hydrogen by the free standing graphene membranes [5] may be evaluated as [14, 21]: ($\Delta H_{(ads.)membr.[5]} - \Delta H_{(des.)membr.[5]}) = -1.5 \pm 0.2$ eV (an exothermic reaction).

One can also suppose that the near-saturation ((C/C_0) $\approx$ 0.95) time ($t_{0.95}$) for the epitaxial graphene samples (at ~300 K) is about 2 h. Hence, by using Eq. (8*) and the above noted data [5] on the relative concentrations (($C_{1h(membr.[5])} / C_{1h(epitax.[5])}) \approx$ 2, and (($C_{3h(membr.[5])} / C_{3h(epitax.[5])}) \approx 3$), one can evaluate the quantities of $\tau_{0.63(epitax.[5])hydr.300K} \approx 0.7$ h and $C_{0(epitax.[5])} \approx 0.16$. Obviously, $C_{0(epitax.[5])}$ is related

only for one of the two sides of an epitaxial graphene layer, and the local atomic ration is (H/C) ≈ 0.19. It is considerably less (about 2.6 times) of the above considered local atomic ratio (H/C) = 0.5 for each of two sides the free standing hydrogenated graphene membranes.

The obtained value of $\tau_{0.63(\text{epitax.}[5])\text{hydr.300K}}$ ≈ 0.7 h (for process of hydrogenation of the epitaxial graphene samples [5]) is much less (by about 2–7 orders) of the evaluated values of the similar quantity for the process of dehydrogenation of the same epitaxial graphene samples [5] ($\tau_{0.63(\text{epitax.}[5])\text{dehydr.300K}}$ ≈ $(1.5 \cdot 10^2 - 1.0 \cdot 10^7)$ h, for $\Delta H_{(\text{des.})}$ = (0.3 − 0.9) eV and $K_{0(\text{des.})}$ = $(0.2 - 3.5 \cdot 10^4)$ s^{-1}, Item 4.2, Table 1A). Hence, by using Eq. 9 and supposing that $K_{0(\text{ads.})} \approx K_{0(\text{des.})}$ (a rough approximation), one can obtain a reasonable value of $\Delta H_{(\text{ads.})\text{epitax.}[5]}$ ≈ 0.3 ± 0.2 eV (Table 1A). The heat of adsorption of atomic hydrogen by the free standing graphene membranes [5] may be evaluated as [14, 21]: ($\Delta H_{(\text{ads.})\text{epitax.}[5]}$ - $\Delta H_{(\text{des.})\text{epitax.}[5]}$) = −0.3 ± 0.2 eV (an exothermic reaction).

The smaller values of $C_{0(\text{epitax.}[5])}$≈0.16 and (H/C)$_{\text{epitax.}[5]}$≈0.19 (in comparison with $C_{0(\text{membr.}[5]\text{one\_side})}$≈0.33 and (H/C)$_{(\text{membr.}[5]\text{one\_side})}$≈0.50) may point to a partial hydrogenation localized in some defected nanoregions [24–34] for the epitaxial graphene samples (even after their prolonged (3 hour) exposures, i.e. after reaching their near-saturation. Similar analytical results, relevance to some other epitaxial graphenes are presented in some next Items.

4.2. Characteristics of dehydrogenation of mono-layer epitaxial graphenes

According to a private communication from D.C. Elias, a near-complete desorption of hydrogen ($-\Delta C/C_0 \approx 0.95$) from a hydrogenated epitaxial graphene on a substrate SiO$_2$ (Fig. 2**A** in [16]) has been achieved by annealing it in 90% Ar/10% H$_2$ mixture at T = 573 K for 2 hours (i.e., $t_{0.95(\text{epitax.}[5])573K}$ = $7.2 \cdot 10^3$ s). Hence, by using Eq. (8), one can evaluate the value of $\tau_{0.63(\text{epitax.}[5])573K}$ = $2.4 \cdot 10^3$ s for the epitaxial graphene [5], which is about six orders less than the evaluated (as in Item 3) value of $\tau_{0.63(\text{membr.}[5])573K}$ = $1.5 \cdot 10^9$ s for the free-standing membranes [5].

The changes in Raman spectra of graphene [5] caused by hydrogenation were rather similar in respect to locations of D, G, D′, 2D and (D+D′) peaks, both for the epitaxial graphene on SiO$_2$ and for the free-standing graphene membrane (Fig. 2 in [16]). Hence, one can suppose that $K_{0(\text{epitax.}[5])}$ = $\nu_{\text{C-H(epitax.}[5])}$ ≈ $K_{0(\text{membr.}[5])}$ = $\nu_{\text{C-}}$

$_{H(membr.[5])} \approx (0.7$ or $5) \cdot 10^{13}$ s^{-1} (Item 3, Table 1A). Then, by substituting in Eq. (9) the values of $K = K_{(epitax.[5])573K} = 1/\tau_{0.63(epitax.[5])573K}$ and $K_0 \approx K_{0(epitax.[5])} \approx K_{0(membr.[5])}$, one can estimate $\Delta H_{des.(epitax.[5])} = \Delta H_{C-H(epitax.[5])} \approx (1.84$ or $1.94)$ eV (Table 1A). Here, the case is supposed of a non-diffusion-rate-limiting kinetics, when Eq. (9) corresponds to the Polanyi-Wigner one [14]. Certainly, these tentative thermodynamic characteristics of the hydrogenated epitaxial graphene on a substrate SiO$_2$ could be directly confirmed and/or modified by further experimental data on $\tau_{0.63(epitax.)}$ at various annealing temperatures.

It is easy to show that: 1) these analytical results (for the epitaxial graphene [5]) are not consistent with the presented below analytical results for the mass spectrometry data (Fig. 3 in [16], TDS peaks ## 1–3, Table 1A) on thermal desorption of hydrogen from a specially prepared single-side (obviously, epitaxial*) graphane [5]; and 2) they cannot be described in the framework of the theoretical models and characteristics of thermal stability of single-side hydrogenated graphene [6] or graphone [9].

According to the further consideration presented below (both in this Item, and in Items 5–11), the epitaxial graphene case ([5] and others) may be related to a hydrogen desorption case of a diffusion rate limiting kinetics, when $K_0 \neq v$, and Eq. (9) does not correspond to the Polanyi-Wigner one [14].

By using the method [14] of treatment of thermal desorption (TDS) spectra, being relevant to the mass spectrometry data [5] (Fig. 3 in [16]) on thermal desorption of hydrogen from the specially prepared single-side (epitaxial*) graphane (under heating from room temperature to 573 K for 6 minutes), one can obtain the following tentative results:

1) the total integrated area of the thermal desorption spectra corresponds to $\sim 10^{-8}$ g of desorbed hydrogen, that may correlate with the graphene layer mass (unfortunately, it's not considered in [5], particularly, for evaluation of the C_0 quantities);

2) the TDS spectra can be approximated by three thermodesorption (TDS) peaks (## 1–3);

3) TDS peak # 1 (~ 30 % of the total area, $T_{max\#1} \approx 370$ K) can be characterized by the activation energy of $\Delta H_{(des.)} = E_{TDS-peak \# 1} = 0.6 \pm 0.3$ eV and by the per-exponential factor of the reaction rate constant $K_{0(TDS-peak \# 1)} \approx 2 \cdot 10^7$ s^{-1};

4) TDS peak # 2 (~15 % of the total area, $T_{max\#2} \approx 445$ K) can be characterized by
the activation energy $\Delta H_{(des.)} = E_{TDS\text{-}peak\ \#\ 2} = 0.6 \pm 0.3$ eV, and by the per-
exponential factor of the reaction rate constant $K_{0(TDS\text{-}peak\ \#\ 2)} \approx 1 \cdot 10^6$ s^{-1};

5) TDS peak # 3 (~55 % of the total area, $T_{max\#3} \approx 540$ K) can be characterized by
the activation energy $\Delta H_{(des.)} = E_{TDS\text{-}peak\ \#\ 3} = 0.23 \pm 0.05$ eV and by the per-
exponential factor of the reaction rate constant $K_{0(TDS\text{-}peak\ \#\ 3)} \approx 2.4$ s^{-1}.

These analytical results (on quantities of $\Delta H_{(des.)}$ and K_0) show that all three of the
above noted thermal desorption (TDS) processes (# 1_{TDS}, # 2_{TDS} and # 3_{TDS}) can not
been described in the framework of the Polanyi-Wigner equation [14, 16] (due to
the obtained low values of the $K_{0(des.)}$ and $\Delta H_{(des.)}$ quantities, in comparison with the
$\nu_{(C\text{-}H)}$ and $\Delta H_{(C\text{-}H)}$ ones).

As is shown below, these results may be related to a hydrogen desorption case of a
diffusion-rate-limiting kinetics [14, 16], when in Eq. 9 the value of $K_0 \approx D_{0app.} / L^2$
and the value of $\Delta H_{des.} = Q_{app.}$, where D_{0app} is the per-exponent factor of the
apparent diffusion coefficient $D_{app.} = D_{0app.}\exp(-Q_{app.}/k_B T)$, $Q_{app.}$ is the apparent
diffusion activation energy, and L is the characteristic diffusion size (length),
which (as is shown below) may correlate with the sample diameter [5] ($L \sim d_{sample} \approx$
$4 \cdot 10^{-3}$ cm, Fig. 2 in [16], Right inset).

TDS process (or peak) # 3_{TDS} (Fig. 3 in [16], Table 1A) may be related to the
diffusion-rate-limiting TDS process (or peak) I in [14], for which the apparent
diffusion activation energy is $Q_{app.I} \approx 0.2$ eV $\approx E_{TDS\text{-}peak\#3}$ and $D_{0app.I} \approx 3 \cdot 10^{-3}$ cm^2/s,
and which is related to chemisorption models "F" and/or "G" (Fig. 4 in [16]).

By supposing of $L \sim d_{sample}$, i.e. of the order of diameter of the epitaxial graphene
specimens [5], one can evaluate the quantity of $D_{0app.(TDS\text{-}peak\#3)} \approx L^2 \cdot K_{0(TDS\text{-}peak\#3)} \approx$
$4 \cdot 10^{-5}$ cm (or within the errors limit, it is of $(1.3–11) \cdot 10^{-5}$ cm, for $E_{TDS\text{-}peak\ \#\ 3}$ values
0.18–0.28 eV, Table 1A). The obtained values of $D_{0app.(TDS\text{-}peak\#3)}$ satisfactory
(within one-two orders, that may be within the errors limit) correlate with the $D_{0app.I}$
quantity. Thus, the above analysis shows that for TDS process (or peak) # 3_{TDS} [5],
the quantity of L may be of the order of diameter (d_{sample}) of the epitaxial* graphene
samples.

Within approach [14], model "F" (Fig. 4 in [16]) is related to a "dissociative-
associative" chemisorption of molecular hydrogen on free surfaces of graphene

layers of the epitaxial samples [5]. Model "G" (Fig. 4 in [16]) is related, within [14] approach, to a "dissociative-associative" chemisorption of molecular hydrogen on definite defects in graphene layers of the epitaxial samples [5], for instance, vacancies, grain boundaries (domains) and/or triple junctions (nodes) of the grain-boundary network [24–34], where the dangling carbon bonds can occur.

TDS processes (or peaks) # 1_{TDS} and # 2_{TDS} [5] (Table 1A) may be (in some extent) related to the diffusion-rate-limiting TDS processes (or peaks) I and II in [14].

Process II is characterized by the apparent diffusion activation energy $Q_{app.II} \approx 1.2$ eV (that is considerably higher of quantities of $E_{TDS-peak\#1}$ and $E_{TDS-peak\#2}$) and $D_{0app.II} \approx 1.8 \cdot 10^3$ cm^2/s. It is related to chemisorption model "H" (Fig. 4 in [16]). Within approach [14], model "H" is related (as and model "G") to a "dissociative – associative" chemisorption of molecular hydrogen on definite defects in graphene layers of the epitaxial samples [5], for instance, vacancies, grain boundaries (domains) and/or triple junctions (nodes) of the grain-boundary network [24–34], where the dangling carbon bonds can occur.

By supposing the possible values of $E_{TDS-peaks\#\#1,2} =$ 0.3, 0.6 or 0.9 eV, one can evaluate the quantities of $K_{0(TDS-peak\#1)}$ and $K_{0(TDS-peak\#2)}$ (Table 1A). Hence, by supposing of $L \sim d_{sample}$, one can evaluate the quantities of $D_{0app.(TDS-peak\#1)}$ and $D_{0app.(TDS-peak\#2)}$, some of them correlate with the $D_{0app.I}$ quantity or with $D_{0app.II}$ quantity. It shows that for TDS processes (or peaks) # 1_{TDS} and # 2_{TDS} [5], the quantity of L may be of the order of diameter of the epitaxial* graphene samples.

For the epitaxial graphene [5] case, supposing the values of $\Delta H_{des.(epitax.[5])} \approx 0.3, 0.6$ or 0.9 eV results in relevant values of $K_{0(epitax.[5])}$ (Table 1A). Hence, by supposing of $L \sim d_{sample}$, one can evaluate the quantities of $D_{0app.(epitax.[5])}$, some of them correlate with the $D_{0app.I}$ quantity or with $D_{0app.II}$ quantity. It shows that for these two processes, the quantity of L also may be of the order of diameter of the epitaxial graphene samples [5].

It is important to note that considered in Items 2 and 3 chemisorption of atomic hydrogen with free-standing graphane-like membranes [5] and with theoretical graphanes [3, 4] may be related to model "F*" considered in [14]. Unlike model "F" (Fig. 4 in [16]), where two hydrogen atoms are adsorbed by two alternated carbon atoms in a graphene-like network, in model "F*" a single hydrogen atom is adsorbed by one of the carbon atoms (in the graphene-like network) possessing of

3 unoccupied (by hydrogen) nearest carbons. Model "F*" is characterized [14] by the quantity of $\Delta H_{(C-H)"F*"} \approx 2.5$ eV, which coincides (within the errors) with the similar quantities ($\Delta H_{(C-H)}$) for graphanes [3–5] (Table 1A). As is also shown in Items 2 and 3, the dehydrogenation processes in graphanes [5, 4] may be the case of a non-diffusion rate limiting kinetics, for which the quantity of K_0 is the corresponding vibration frequency ($K_0 = \nu$), and Eq. (9) is correspond to the Polanyi-Wigner one [14, 16].

On the other hand, model "F*" is manifested in the diffusion-rate-limiting TDS process (or peak) III in [14] (Table 1B), for which the apparent diffusion activation energy is $Q_{app.III} \approx 2.6$ eV $\approx \Delta H_{(C-H)"F*"}$ and $D_{0app.III} \approx 3 \cdot 10^{-3}$ cm^2/s. Process III is relevant to a dissociative chemisorption of molecular hydrogen between graphene-like layers in graphite materials (isotropic graphite and nanostructured one) and nanomaterials (graphite nanofibers) [14] (Table 1B).

It is expedient also to note about models "C" and "D", those are manifested in the diffusion-rate-limiting TDS process (or peak) IV in [14] (Table 1B), for which the apparent diffusion activation energy is $Q_{app.IV} \approx 3.8$ eV $\approx \Delta H_{(C-H)"C","D"}$ and $D_{0app.IV} \approx 6 \cdot 10^2$ cm^2/s. Process IV is relevant to a dissociative chemisorption of molecular hydrogen in defected regions in graphite materials (isotropic graphite, pyrolytic graphane and nanostructured one) [14] (Table 1B).

But such processes (III and IV) have not manifested, when the thermal desorption annealing of the hydrogenated epitaxial graphene samples [5] (Fig. 3 in [16]), unlike some hydrogen sorption processes in epitaxial graphenes and graphite samples considered in some next Items.

4.3. An interpretation of hydrogenation-dehydrogenation characteristics of mono-layer epitaxial graphenes

The above obtained values (Item 4.2, Tables 1A, 1B) of dehydrogenation characteristics of mono-layer epitaxial graphene samples [5] can be presented, as follows: $\Delta H_{des.} \sim Q_{app.I}$ or $\sim Q_{app.II}$ [14], $K_{0(des.)} \sim (D_{0app.I} / L^2)$ or $\sim (D_{0app.II} / L^2)$ [14], $L \sim d_{sample}$, i.e. being of the order of diameter of the epitaxial graphene samples [5]. And it is related to the chemisorption models "F", "G" and/or "H" (Fig. 4 in [16]).

These characteristics unambiguously point that in the epitaxial graphene samples [5], there are the rate-limiting processes (types of I and/or II [14]) of diffusion of hydrogen, mainly, from chemisorption "centers" (of "F", "G" and/or "H" types (Fig. 4 in [16])) localized on the internal graphene surfaces (and/or in the graphene/substrate interfaces) to the frontier edges of the samples. It corresponds to the characteristic diffusion length ($L \sim d_{sample}$) of the order of diameter of the epitaxial graphene samples, which, obviously, can not be manifested for a case of hydrogen desorption processes from the external graphene surfaces. Such interpretation is direct opposite, relevance to the interpretation of authors [5] and a number of others, those probably believe in occurrence of hydrogen desorption processes, mainly, from the external epitaxial graphene surfaces.

Such different (in some sense, extraordinary) interpretation is consisted with the above analytical data (Item 4.1, Table 1A) on activation energies of hydrogen adsorption for the epitaxial graphene samples ($\Delta H_{(ads.)epitax.[5]} \approx 0.3 \pm 0.2$ eV), which is much less than the similar one for the free standing graphene membranes [5] ($\Delta H_{(ads.)membr.[5]} = 1.0 \pm 0.2$ eV). It may be understood for the case of chemisorotion (of "F", "G" and/or "H" types (Fig. 4 in [16])) on the internal graphene surfaces (neighboring to the substrate (SiO_2) surfaces), which obviously proceeds without the diamond-like strong distortion of the graphene network, unlike graphane [3] (Item 1).

Such an extraordinary interpretation is also consisted with the above analytical results (Item 4.1) about the smaller values of $C_{0(epitax.[5])} \approx 0.16$ and $(H/C)_{(epitax.[5])} \approx 0.19$, in comparison with $C_{0(membr.[5]one\_side)} \approx 0.33$ and $(H/C)_{(membr.[5]one\_side)} \approx 0.50$. It may point to an "internal" (in the above considered sense) local hydrogenation in the epitaxial graphene layers. It may be, for instance, an "internal" hydrogenation localized, mainly, in some defected nanoregions [24–34] mentioned above (Items 1, 4.2), where their near-saturation may be reached after prolonged (3 hour) exposures.

On the basis of the above analytical results, one can suppose that a negligible hydrogen adsorption by the external graphene surfaces (in the epitaxial samples [5]) is exhibited. Such situation may be due to a much higher rigidity of the epitaxial graphenes (in comparison with the free standing graphene membranes), that may suppress the diamond-like strong distortion of the graphene network attributed for graphane [3] (Item 1). It may result (for the epitaxial graphenes [5]) in disappearance of the hydrogen chemisorption with characteristics of

$\Delta H_{(ads.)membr.[5]}$ and $\Delta H_{(des.)membr.[5]}$ (Table 1A) manifested in the case of the free standing graphene membranes [5]. And the hydrogen chemisorption with characteristics of $\Delta H_{(ads.)epitax.[5]}$ and ($\Delta H_{(des.)epitax.[5]}$ (Table 1A) by the external graphene surfaces, in the epitaxial samples [5], is not observed, may be, due to a very fast desorption kinetics, unlike the kinetics in the case of the internal graphene surfaces.

Certainly, such an extraordinary interpretation also needs in a reasonable explanation of results (Fig. 2 in [16]) the fact that the changes in Raman spectra of graphene [5] caused by hydrogenation were rather similar with respect to locations of D, G, D′, 2D and (D+D′) peaks, both for the epitaxial graphene on SiO_2 and for the free-standing graphene membrane.

4.4. An interpretation of the data on hydrogenation of bi-layer epitaxial graphenes

In work [5], the same hydrogenation procedures of the 2 hour long expositions have been applied also for bi-layer epitaxial graphene on SiO_2/Si wafer. Bi-layer samples showed little change in their charge carrier mobility and a small D Raman peak, compared to the single-layer epitaxial graphene on SiO_2/Si wafer exposed to the same hydrogenation procedures. The authors [5] believe that higher rigidity of bi-layers suppressed their rippling, thus reducing the probability of hydrogen adsorption.

But such an interpretation [5] seems not enough adequate, if the above (Item 4.3) and below (next Items) presented consideration and interpretation of a number of data are taken into account.

By using the above extraordinary interpretation (Item 4.3) and results on characteristics ($Q_{app.III} \approx 2.6$ eV, $D_{0app.III} \approx 3 \cdot 10^{-3}$ cm^2/s (Item 4.2, Table 1B) of a rather slow diffusion of atomic hydrogen between neighboring graphene-like layers in graphitic materials and nanostructures (process III, model "F*" [14]), one can suppose a negligible diffusion penetration of atomic hydrogen between the two graphene layers in the bi-layer epitaxial samples [5] (during the hydrogenation procedures of the 2 hour long expositions, obviously, at $T \approx 300$ K). Indeed, by using values of $Q_{app.III}$ and $D_{0app.III}$, one can estimate the characteristic diffusion size (length) $L \sim 7 \cdot 10^{-22}$ cm, which points to absence of such diffusion penetration.

In the next Items of this study, a further consideration of some other known experimental data on hydrogenation and thermal stability characteristics of mono-layer, bi-layer and three-layer epitaxial graphene systems is given, where (as is there shown) an important role plays some defects found in graphene networks [24–34], relevant to the probability of hydrogen adsorption and the permeability of graphene networks for atomic hydrogen (Item 1).

5. Consideration and interpretation of the Raman spectroscopy data [35] on hydrogenation-dehydrogenation of graphene flakes

In [35], it is reported that the hydrogenation of single and bilayer graphene flakes by an argon-hydrogen plasma produced a reactive ion etching (RIE) system. They analyzed two cases: one where the graphene flakes were electrically insulated from the chamber electrodes by the SiO_2 substrate, and the other where the flakes were in electrical contact with the source electrode (a graphene device). Electronic transport measurements in combination with Raman spectroscopy were used to link the electric mean free path to the optically extracted defect concentration, which is related to the defect distance ($L_{def.}$). This shows that under the chosen plasma conditions, the process does not introduce considerable damage to the graphene sheet, and that a rather partial hydrogenation ($C_H \leq 0.05\%$) occurs primarily due to the hydrogen ions from the plasma, and not due to fragmentation of water adsorbates on the graphene surface by highly accelerated plasma electrons. To quantify the level of hydrogenation, they used the integrated intensity ratio (I_D/I_G) of Raman bands. The hydrogen coverage (C_H) determined from the defect distance ($L_{def.}$) did not exceed $\sim 0.05\%$.

Table 2

Analytical quantities related to Items 5–7, comparing with ones of Items 1–4

Material	Value/Quantity		
	$\Delta H_{(des.)}$, eV $\{\Delta H_{(ads.)}$, eV$\}$	$K_{0(des.)}$, s^{-1} $\{L \approx (D_{0app.III}/K_{0(des.)})^{1/2}\}$	$\tau_{0.63(des.)553K}$, s $\{\tau_{0.63(ads.)300K}$, s$\}$
Graphene flakes/SiO$_2$ [35]	0.11 ± 0.07 (as process ⊔ I [14], ⊔ models "F", "G", Fig.4 in [16]) $\{0.1 \pm 0.1\}$	0.15 (for 0.11 eV) $\{L \sqsubset d_{sample}\}$	$7\cdot 10^3$ $\{9\cdot 10^4\}$
Graphene/Ni [36-38] HOPG [36-38]			$1.3\cdot 10^2 - 2.6\cdot 10^2$ $\{5\cdot 10^4 - 1.0\cdot 10^3\}$ $1.3\cdot 10^2 - 2.6\cdot 10^2$ $\{5\cdot 10^4 - 1.0\cdot 10^3\}$

(SiC-D/QFMLG-H) [39]	0.7 ± 0.2 (as processes ⊔ I-II [14], ⊔ model "G", Fig.4 in [16])	$9 \cdot 10^2$ (for 0.7 eV) {L ⊔ d_{sample}}	$2.7 \cdot 10^3$
(SiC-D/QFMLG) [39]	2.0 ± 0.6 2.6 (as process ⊔ III [14], ⊔ model "F*")	$1 \cdot 10^6$ (for 2.0 eV) $6 \cdot 10^8$ (for 2.6 eV) {$L \approx 22$ nm}	$1.7 \cdot 10^{12}$ $8 \cdot 10^{14}$
Graphene/SiO₂ [5] (Table 1A)	If 0.3 if 0.6 if 0.9 (as processes ⊔ I-II [14], ⊔ model "G", Fig.4 in [16]) {0.3 ± 0.2}	then 0.2 then $0.8 \cdot 10^2$ then $3.5 \cdot 10^4$ {L ⊔ d_{sample}}	$0.3 \cdot 10^2$ $3.7 \cdot 10^3$ $4.6 \cdot 10^3$ {$2.5 \cdot 10^3$} Item 4.1
Graphene*/SiO₂ (TDS-peak #3) [5] (Table 1A)	0.23 ± 0.05 (as process ⊔ I [14], ⊔ models "F", "G", Fig.4 in [16])	2.4 (for 0.23 eV) {L ⊔ d_{sample}}	$5 \cdot 10^3$
Graphene*/SiO₂ (TDS-peak #2) [5] (Table 1A)	0.6 ± 0.3 (as processes ⊔ I-II [14], ⊔ model "G", Fig.4 in [16])	$1 \cdot 10^6$ (for 0.6 eV) {L ⊔ d_{sample}}	0.3
Graphene*/SiO₂ (TDS-peak #1) [5] (Table 1A)	0.6 ± 0.3 (as processes ⊔ I-II [14], ⊔ model "G", Fig.4 in [16])	$2 \cdot 10^7$ (for 0.6 eV) {L ⊔ d_{sample}}	$1.5 \cdot 10^{-2}$

In [16], the data [35] (Fig. 5 in [16]) have been treated and analyzed. The obtained analytical results (Table 2) on characteristics of hydrogenation-dehydrogenation of graphene flakes [35] may be interpreted within the models used in Item 4 for interpretation of the similar characteristics for the epitaxial graphenes [5] (Table 1A), which are also presented (for comparing) in Table 2.

By taking into account the facts that the REI exposure regime [35] is characterized by a form of $(I_D/I_G) \sim L_{def.}^{-2}$ (for $(I_D/I_G) < 2.5$), $L_{def.} \approx 11 - 17$ nm and the hydrogen concentration $C_H \leq 5 \cdot 10^{-4}$, one can suppose that the hydrogen adsorption centers in the single graphene flakes (on the SiO₂ substrate) are related to some point nanodefects (i.e., vacancies and/or triple junctions (nodes) of the grain-boundary network) of diameter $d_{def.} \approx$ const. In such a model, the quantity C_H can be described satisfactory as:

$$C_H \approx n_H (d_{def.})^2 / (L_{def.})^2, \qquad (10)$$

where $n_H \approx$ const. is the number of hydrogen atoms adsorbed by a center; $C_H \sim (I_D/I_G) \sim L_{def.}^{-2}$.

It was also found [35] that after the Ar/H$_2$ plasma exposure, the (I_D/I_G) ratio for bi-layer graphene device is larger than that of the single graphene device. As noted in [35], this observation is in contradiction to the Raman ratios after exposure of graphene to atomic hydrogen and when other defects are introduced. Such a situation may have place in [5] for bi-layer epitaxial graphene on SiO$_2$/Si wafer (Item 4.4).

6. Consideration and interpretation of the STM/STS data [36] on hydrogenation-dehydrogenation of epitaxial graphene and graphite (HOPG) surfaces

In [36], the effect of hydrogenation on topography and electronic properties of graphene grown by CVD on top of a nickel surface and high oriented pyrolytical graphite (HOPG) surfaces were studied by scanning tunneling microscopy (STM) and spectroscopy (STS). The surfaces were chemically modified using 40 min Ar/H$_2$ plasma (with 3 W power) treatment (Fig. 6 in [16]). This determines that the hydrogen chemisorption on the surface of graphite/graphene opens on average an energy bandgap of 0.4 eV around the Fermi level. Although the plasma treatment modifies the surface topography in an irreversible way, the change in the electronic properties can be reversed by moderate thermal annealing (for 10 min at 553 K), and the samples can be hydrogenated again to yield a similar, but slightly reduced, semiconducting behavior after the second hydrogenation.

The data (Fig. 6 in [16]) show that the time of desorption from both the epitaxial graphene/Ni samples and HOPG samples of about 90–99% of hydrogen under 553 K annealing is $t_{0.9(des.)553K}$ (or $t_{0.99(des.)553K}$) $\approx 6 \cdot 10^2$ s. Hence, by using Eq. (8), one can estimate the quantity $\tau_{0.63(des.)553K[52]} \approx 260$ (or 130) s, which is close (within the errors) to the similar quantity of $\tau_{0.63(des.)553K[51]} \approx 70$ s for the epitaxial graphene flakes [35] (Table 2).

The data (Fig. 6 in [16]) also show that the time of adsorption (for both the epitaxial graphene/Ni samples and HOPG samples) of about 90–99% of the saturation hydrogen amount (under charging at about 300 K) is $t_{0.9(ads.)300K}$ (or $t_{0.99(ads.)300K}$) $\approx 2.4 \cdot 10^3$ s. Hence, by using Eq. (8*), one can estimate the quantity $\tau_{0.63(ads.)300K[52]} \approx (1.1$ or $0.5) \cdot 10^2$ s, which coincides (within the errors) with the similar quantity of $\tau_{0.63(ads.)300K[51]} \approx 9 \cdot 10^2$ s for the epitaxial graphene flakes [35] (Table 2).

The data (Fig. 6 in [16]) also show that the time of adsorption (for both the epitaxial graphene/Ni samples and HOPG samples) of about 90–99% of the saturation hydrogen amount (under charging at about 300 K) is $t_{0.9(ads.)300K}$ (or $t_{0.99(ads.)300K}$) $\approx 2.4 \cdot 10^3$ s. Hence, by using Eq. (8*), one can estimate the quantity $\tau_{0.63(ads.)300K[52]} \approx (1.1$ or $0.5) \cdot 10^2$ s, which coincides (within the errors) with the similar quantity of $\tau_{0.63(ads.)300K[51]} \approx 9 \cdot 10^2$ s for the epitaxial graphene flakes [35] considered in the previous Item (Table 2).

These analytical results on characteristics of hydrogenation-dehydrogenation of epitaxial graphene and graphite surfaces [37] (also as the results for graphene flakes [35] presented in the previous Item) may be interpreted within the models used in Item 4 for interpretation of the similar characteristics for the epitaxial graphenes [5] (Tables 1, 2).

As is noted in [37], before the plasma treatment, the CVD graphene exhibits a Moiré pattern superimposed to the honeycomb lattice of graphene (Fig. 6(d) in [16]). This is due to the lattice parameter mismatch between the graphene and the nickel surfaces, and thus the characteristics of the most of the epitaxial graphene samples. On the other hand, as is also noted in [37], for the hydrogenated CVD graphene, the expected structural changes are twofold. First, the chemisorption of hydrogen atoms will change the sp^2 hybridization of carbon atoms to tetragonal sp^3 hybridization, modifying the surface geometry. Second, the impact of heavy Ar ions, present in the plasma, could also modify the surface by inducing geometrical displacement of carbon atoms (rippling graphene surface) or creating vacancies and other defects (for instance, grain or domain boundaries [24–34]). Fig. 6(e) in [16] shows the topography image of the surface CVD graphene after the extended (40 min) plasma treatment. The nano-order-corrugation increases after the treatment, and there are brighter nano-regions (of about 1 nm in height and several nm in diameter) in which the atomic resolution is lost or strongly distorted. It was also found [36, 37] that these bright nano-regions present a semiconducting behavior, while the rest of the surface remains conducting (Fig. 6(g)-(h) in [16]).

It is reasonable to assume that most of the chemisorbed hydrogen is localized into these bright nano-regions, which have a blister-like form. Moreover, it is also reasonable to assume that the monolayer (single) graphene flakes on the Ni substrate are permeable to atomic hydrogen only in these defected nano-regions. This problem has been formulated in Item 1 (Introduction). A similar model may be valid and relevant for the HOPG samples (Fig. 6 (a) – (c) in [16]).

It has been found out that when graphene is deposited on a SiO_2 surface (Figs. 7, 8 in [16]), the charged impurities presented in the graphene/substrate interface produce strong inhomogeneities of the electronic properties of graphene. On the other hand, it has also been shown how homogeneous graphene grown by CVD can be altered by chemical modification of its surface by the chemisoption of hydrogen. It strongly depresses the local conductance at low biases, indicating the opening of a band gap in graphene [37, 38].

The charge inhomogeneities (defects) of epitaxial hydrogenated graphene/ SiO_2 samples do not show long range ordering, and the mean spacing between them is $L_{def.} \approx 20$ nm (Fig. 8 in [16]). It is reasonable to assume that the charge inhomogeneities (defects) are located at the interface between the SiO_2 layer (300 nm thick) and the graphene flake [37, 38]. A similar quantity ($L_{def.} \approx 11 - 17$ nm, [35])) for the hydrogen adsorption centers in the monolayer graphene flakes on the SiO_2 substrate has been considered in Item 5.

7. Consideration and interpretation of the HREELS/LEED data [39] on dehydrogenation of epitaxial graphene on SiC substrate

In [39], hydrogenation of deuterium-intercalated quasi-free-standing monolayer graphene on SiC(0001) was obtained and studied with low-energy electron diffraction (LEED) and high-resolution electron energy loss spectroscopy (HREELS). While the carbon honeycomb structure remain(ed) intact, it has shown a significant band gap opening in the hydrogenated material. Vibrational spectroscopy evidences for hydrogen chemisorption on the quasi-free-standing graphene has been provided and its thermal stability has been studied (Fig. 9 in [16]). Deuterium intercalation, transforming the buffer layer in quasi-free-standing monolayer graphene (denoted as SiC-D/QFMLG), has been performed with a D atom exposure of $\sim 5 \cdot 10^{17}$ cm^{-2} at a surface temperature of 950 K. Finally, hydrogenation up to saturation of quasi-free-standing monolayer graphene has been performed at room temperature with a H atom exposure $> 3 \cdot 10^{15}$ cm^{-2}. The latter sample has been denoted as SiC-D/QFMLG-H to stress the different used isotopes.

According to a private communication from R. Bisson, the temperature indicated at each point in Fig. 9 in [16] corresponds to successive temperature ramp (not linear) of 5 minutes. Within a formal kinetics approach for the first order reactions [14,

21], one can treat the above noted points at T_i = 543 K, 611 K and 686 K, by using
Eq. (8) transformed to a more suitable form (8′): $K_i \approx -(ln(C/C_{0i})/t)$, where t = 300
s, and the corresponding quantities C_{0i} and C are determined from Fig. 9 in [16]. It
led to finding values of the reaction (hydrogen desorption from SiC-D/QFMLG-H
samples) rate constant $K_{i(des.)}$ for 3 temperatures T_i = 543, 611 and 686 K. The
temperature dependence is described by Eq. (9). Hence, the desired quantities have
been determined (Table 2) as the reaction (hydrogen desorption) activation energy
$\Delta H_{(des.)(SiC-D/QFMLG-H)[55]}$ = 0.7 ± 0.2 eV, and the per-exponential factor of the
reaction rate constant $K_{0(des.)(SiC-D/QFMLG-H)[55]} \approx 9 \cdot 10^2$ s^{-1}. The obtained value of
$\Delta H_{(des.)(SiC-D/QFMLG-H)[55]}$ is close (within the errors) to the similar ones ($E_{TDS-peak \# 1[5]}$
and $E_{TDS-peak \# 2[5]}$) for TDS processes # 1 and # 2 (Item 4.2, Table 1A). But the
obtained value $K_{0des.(SiC-D/QFMLG-H)[55]}$ differs by several orders from the similar ones
($K_{0des.(TDS-peak \# 1)[5]}$ and $K_{0des.(TDS-peak \# 2)[5]}$) for TDS processes # 1 and # 2 (Item 4.2,
Table 1A). Nevertheless, these three desorption processes may be (in some extent)
related to chemisorption models "H" and/or "G" (Fig. 4 in [16]).

These analytical results on characteristics of hydrogen desorption (dehydroge-
nation) from (of) SiC-D/QFMLG-H samples [39] may be also (as the results from
Items 5 and 6) interpreted within the models used in Item 4 for interpretation of the
similar characteristics for the epitaxial graphenes [5] (Tables 1A, 2).

In the same way, one can treat the points from Fig. 9 in [16] (at T_i = 1010, 1120
and 1200 K), which are related to the intercalated deuterium desorption from SiC-
D/QFMLG samples. This led to finding the desired quantities (Table 2): the
reaction (deuterium desorption) activation energy $\Delta H_{(des.)(SiC-D/QFMLG)[55]}$ = 2.0 ± 0.6
eV, and the per-exponential factor of the reaction rate constant $K_{0(des.)(SiC-D/QFMLG)[55]}$
$\approx 1 \cdot 10^6$ s^{-1}.

Such a relatively low (in comparison with the vibration C-H or C-D frequencies)
value of $K_{0(des.)(SiC-D/QFMLG)[55]}$ points to that the process can not be described within
the Polanyi-Wigner model [14, 16] related the case of a non-diffusion rate limiting
kinetics.

And as is concluded in [39], the exact intercalation mechanism of hydrogen
diffusion through the anchored graphene lattice, at a defect or at a boundary of the
anchored graphene layer, remains an open question.

Formally, this desorption process (obviously, of a diffusion-limiting character) may be described (as is shown below) similarly to TDS process III (model "F*") in [14] (Table 1B), and the apparent diffusion activation energy may be close to the break-down energies of the C-H bonds.

Obviously that such analytical results on characteristics of deuterium desorption from SiC-D/QFMLG samples [39] may not be interpreted within the models used in Item 4 for interpretation of the similar characteristics for the epitaxial graphenes [5] (Tables 1A, 2).

But these results (for SiC-D/QFMLG samples [39]) may be quantitatively interpreted on the basis of using the characteristics of process III in [14] noted in Item 4.2 (Table 1B). Indeed, by using the quantities' values (from Table 1) of $\Delta H_{(des.)(SiC-D/QFMLG)[55]} \approx Q_{app.III} \approx 2.6$ eV, $K_{0(des.)(SiC-D/QFMLG)[55]} \approx 6\cdot10^8$ s^{-1} and $D_{0app.III} \approx 3\cdot10^{-3}$ cm^2/s, one can estimate the quantity of $L \approx (D_{0app.III} / K_{0(des.)})^{1/2} = 22$ nm. The obtained value of L coincides (within the errors) with values of the quantities of $L_{def.} \approx 11 - 17$ nm (Item 5, Eq. (10)) and $L_{def.} \approx 20$ nm (Item 6, Fig. 8(b) in [16]). It shows that in the case under consideration, the intercalation mechanism of hydrogen (deuterium) diffusion through the anchored graphene lattice at the corresponding point type defects [24–34] of the anchored graphene layer may have place. And the desorption process of the intercalated deuterium may be rate-limited by diffusion of deuterium atoms to a nearest one of such point type defects of the anchored graphene layer.

It is reasonable to assume that the quasi-free-standing monolayer graphene on the SiC-D substrate is permeable to atomic hydrogen (at room temperature) in some defect nano-regions (probably, in vacancies and/or triple junctions (nodes) of the grain-boundary network [24–34]).

It would be expedient to note that the HREELS data [39] on bending and stretching vibration C-H frequencies in SiC-D/QFMLG-H samples (153 meV ($3.7\cdot10^{13}$ s^{-1}) and 331 meV ($8.0\cdot10^{13}$ s^{-1}), respectively) are consistent with those [23] considered in Items 3, related to the HREELS data for the epitaxial graphene [5].

The obtained characteristics (Table 2) of desorption processes [35–39] show that all these processes may be of a diffusion-rate-controlling character [14].

8. Consideration and interpretation of the Raman spectroscopy data [40] on dehydrogenation of graphene layers on SiO₂ substrate

In [40], graphene layers on SiO_2/Si substrate have been chemically decorated by radio frequency hydrogen plasma (the power of 5–15 W, the pressure of 1 Tor) treatment for 1 min. The investigation of hydrogen coverage by Raman spectroscopy and micro-x-ray photoelectron spectroscopy characterization demonstrates that the hydrogenation of a single layer graphene on SiO_2/Si substrate is much less feasible than that of bilayer and multilayer graphene. Both the hydrogenation and dehydrogenation processes of the graphene layers are controlled by the corresponding energy barriers, which show significant dependence on the number of layers. These results [40] on bilayer graphene/SiO_2/Si are in contradiction to the results [5] on a negligible hydrogenation of bi-layer epitaxial graphene on SiO_2/Si wafer, when obviously other defects are produced.

Within a formal kinetics approach [14, 21], the kinetic data (from Fig. 10 (a) in [16]) for single layer graphene samples (1LG-5W and 1LG-15W ones) can be treated. Eq. (7) is used to transform into a more suitable form (7′): $K \approx -((\Delta C/\Delta t)/C)$, where $\Delta t = 1800$ s, and ΔC and C are determined from Fig. 10 (a) in [16].

The results have been obtained for 1LG-15W sample 3 values of the # 1 reaction rate constant $K_{1(1LG-15W)}$ for 3 temperatures ($T = 373$, 398 and 423 K), and 3 values of the # 2 reaction rate constant $K_{2(1LG-15W)}$ for 3 temperatures ($T = 523$, 573 and 623 K). Hence, by using Eq. (9), the following quantities for 1LG-15W samples have been determined (Table 3): the # 1 reaction activation energy $\Delta H_{des.1(1LG-15W)} = 0.6 \pm 0.2$ eV, the per-exponential factor of the # 1 reaction rate constant $K_{0des.1(1LG-15W)} \approx 2 \cdot 10^4$ s⁻¹, the # 2 reaction activation energy $\Delta H_{des.2[(1LG-15W)} = 0.19 \pm 0.07$ eV, and the per-exponential factor of the # 2 reaction rate constant $K_{0des.2[(1LG-15W)} \approx 3 \cdot 10^{-2}$ s⁻¹.

It also led to finding for 1LG-5W sample 4 values of the # 1 reaction rate constant $K_{I(1LG-5W)}$ for 4 temperatures ($T = 348$, 373, 398 and 423 K), and 2 values of the # 2 reaction rate constant $K_{2(1LG-5W)}$ for 2 temperatures ($T = 523$ and 573 K). Therefore by using Eq. (9), one can evaluate the desired quantities for 1LG-5W specimens (Table 3): the # 1 reaction activation energy $\Delta H_{des.1(1LG-5W)} = 0.15 \pm 0.04$ eV, the per-exponential factor of the # 1 reaction rate constant $K_{0des.1[(1LG-5W)} \approx 2 \cdot 10^{-2}$ s⁻¹, the # 2 reaction activation energy $\Delta H_{des.2(1LG-5W)} = 0.31 \pm 0.07$ eV, and the per-exponential factor of the # 2 reaction rate constant $K_{0des.2(1LG-5W)} \approx 0.5$ s⁻¹.

A similar treatment of the kinetic data (from Fig. 10 (c) in [16]) for bilayer graphene 2LG-15W samples led to obtaining 4 values of the # 2 reaction rate constant $K_{2(2LG-15W)}$ for 4 temperatures (T = 623, 673, 723 and 773 K). Hence, by using Eq. (9), the following desired values are found (Table 3): the # 2 reaction activation energy $\Delta H_{des.2(2LG-15W)}$ = 0.9 ± 0.3 eV, the per-exponential factor of the # 2 reaction rate constant $K_{0des.2(2LG-15W)} \approx 1 \cdot 10^3$ s^{-1}.

A similar treatment of the kinetic data (from Fig. 6 (c) in [56]) for bilayer graphene 2LG-5W samples led to obtaining 4 values for the # 1 reaction rate constant $K_{1(2LG-5W)}$ for 4 temperatures (T = 348, 373, 398 and 423 K), and 3 values for the # 2 reaction rate constant $K_{2(2LG-5W)}$ for 3 temperatures (T = 573, 623 and 673 K). Their temperature dependence is described by Eq. (9). Hence, one can evaluate the following desired values (Table 3): the # 1 reaction activation energy $\Delta H_{des.1[(2LG-5W)}$ = 0.50 ± 0.15 eV, the per-exponential factor of the # 1 reaction rate constant $K_{0des.1(2LG-5W)} \approx 2 \cdot 10^3$ s^{-1}, the # 2 reaction activation energy $\Delta H_{des.2(2LG-5W)}$ = 0.40 ± 0.15 eV, and the per-exponential factor of the # 2 reaction rate constant $K_{0des.2(2LG-5W)} \approx 1$ s^{-1}.

The obtained analytical results (Table 3) on characteristics of the desorption (dehydrogenation) processes # 1 and # 2 [40] may be interpreted within the models used in Item 4 for interpretation of the similar characteristics for the epitaxial graphenes [5] (Table 1A). It shows that the desorption processes # 1 and # 2 (in [40]) may be of a diffusion-rate-controlling character.

Table 3

Some analytical results of Items 8-11

Samples	Values / Quantities			
	$\Delta H_{(des.)1}$ (eV)	$K_{0(des.)1}$ (s^{-1}) {L}	$\Delta H_{(des.)2}$ (eV)	$K_{0(des.)2}$ (s^{-1}) {L}
1LG-15W (graphene) [40]	0.6 ± 0.2 (as processes I-II [14], model "G", Fig. 4 in [16])	$2 \cdot 10^4$ {L d_{sample}}	0.19 ± 0.07 (as process I [14], models "F", "G", Fig. 4 in [16])	$3 \cdot 10^{-2}$ {L d_{sample}}
2LG-15W (bi-graphene) [40]			0.9 ± 0.3 (as processes I-II [14], model "G", Fig.4 in [16])	$1 \cdot 10^3$ {L d_{sample}}
1LG-5W (graphene) [40]	0.15 ± 0.04 (as process I [14], models "F","G", Fig. 4 in [16])	$2 \cdot 10^{-2}$ {L d_{sample}}	0.31 ± 0.07 (as process I [14], models	$5 \cdot 10^{-1}$ {L d_{sample}}

			"F","G", Fig.4 in [16])	
2LG-5W (bi-graphene) [40]	0.50 ± 0.15 (as processes I-II [14], model"G", Fig. 4 in [16])	$2 \cdot 10^3$ {L d_{sample}}	0.40 ± 0.15 (as processes I-II [14], model"G", Fig. 4 in [16])	1.0 {L d_{sample}}
HOPG [41], TDS-peaks 1, 2	0.6 ± 0.2 (as processes I-II [14], model "G", Fig.4 in [16])	$1.5 \cdot 10^4$ {L d_{sample}}	1.0 ± 0.3 (as processes I-II [14], model "G", Fig. 4 in [16])	$2 \cdot 10^6$ {L d_{sample}}
Graphene/SiC [43]			3.6 (as process IV [14], models "C","D", Fig. 4 in [16])	$2 \cdot 10^{14}$ $\nu_{(C-H)}$ {L 17nm}
HOPG [45], TDS-peaks 1, 2 HOPG [45], TDS-peak 1	2.4 [45] (as process III [14], model "F*") 2.4 ± 0.5 (as process III [14], model "F*")	$2 \cdot 10^{10}$ {L 4 nm}	4.1 [45] (as process IV [14], models "C", "D", Fig. 4 in [16])	

9. Consideration and interpretation of the TDS/STM data [41] for HOPG treated by atomic deuterium

In [41], the results are presented of a scanning tunneling microscopy (STM) study of HOPG (high oriented pyrolytical graphite) samples treated by atomic deuterium, which reveals the existence of two distinct hydrogen dimer nano-states on graphite basal planes (Figs. 11 and 12 (b) in [16]). The density functional theory calculations allow them to identify the atomic structure of these nano-states and to determine their recombination and desorption pathways. As predicted, the direct recombination is only possible from one of the two dimer nano-states. In conclusion [41], this results in an increased stability of one dimer nanospecies, and explains the puzzling double peak structure observed in temperature programmed desorption spectra (TPD or TDS) for hydrogen on graphite (Fig. 12 (a) in [16]).

By using the method [14] of TDS peaks' treatment, for the case of TDS peak 1 ($\sim$65 % of the total area, $T_{max\#1} \approx 473$ K) in Fig. 12(a) in [16], one can obtain values of the reaction # 1 rate constant ($K_{(des.)1} = 1/\tau_{0.63(des.)1}$) for several temperatures (for instance, $T = 458$, 482 and 496 K). Their temperature dependence can be described by Eq. (9). Hence, the desired values are defined as follows (Table 3): the # 1 reaction (desorption) activation energy $\Delta H_{(des.)1} = 0.6 \pm 0.2$ eV, and the per-exponential factor of the # 1 reaction rate constant $K_{0(des.)1} \approx 1.5 \cdot 10^4$ s^{-1}.

In a similar way, for the case of TDS peak 2 (~35 % of the total area, $T_{max\#2} \approx 588$ K)) in Fig. 12(a) in [16], one can obtain values of the # 2 reaction rate constant ($K_{(des.)2} = 1/\tau_{0.63(des.)2}$) for several temperatures (for instance, $T = 561$ and 607 K). Hence, the desired values are defined as follows (Table 3): the # 2 reaction (desorption) activation energy $\Delta H_{(des.)2} = 1.0 \pm 0.3$ eV, and the per-exponential factor of the # 2 reaction rate constant $K_{0(des.)2} \approx 2 \cdot 10^6$ s^{-1}.

The obtained analytical results (Table 3) on characteristics of the desorption (dehydrogenation) processes # 1 and # 2 in [41] (also as in [40], Item 8) may be interpreted within the models used in Item 4 for interpretation of the similar characteristics for the epitaxial graphenes [5] (Table 1A). It shows that the desorption processes # 1 and # 2 (in [41] and [40]) may be of a diffusion-rate-controlling character. Therefore, these processes can not be described by using the Polanyi-Wigner equation (as it has been done in [41]).

The observed "dimer nano-states" or "nano-protrusions" (Figs. 11 and 12(b) in [16] (from [41])) may be related to the defected nano-regions, probably, as grain (domain) boundaries [24–34] and/or triple and other junctions (nodes) of the grain-boundary network in the HOPG samples. Some defected nano-regions at the grain boundary network (hydrogen adsorption centres # 1, mainly, the "dimer B" nano-structures) can be related to TPD (TDS) peak 1, the others (hydrogen adsorption centres # 2, mainly, the "dimer A" nano-structures) to TPD (TDS) peak 2.

In Figs. 11(a) and 12(b) in [16] (from [41]), one can imagine some grain boundary network (with the grain size of about 2–5 nm) decorated (obviously, in some nano-regions at grain boundaries) by some bright nano-protrusions. Similar "nano-protrusions" are observed and in graphene/SiC systems [42, 43] (Figs. 13–16 in [16]).

In [42], hydrogenation was studied by a beam of atomic deuterium 10^{12}-10^{13} cm^{-2}s^{-1} (corresponding to $P_D \approx 10^{-4}$ Pa) at 1 600 K, and the time of exposure of 5–90 s, for single graphene on SiC-substrate. The formation of graphene blisters were observed, and intercalated with hydrogen in them (Figs. 13 and 14 in [16]), similar to those observed on graphite [41] (Figs. 11 and 12 in [16]) and graphene/SiO$_2$ [43] (Figs. 15 and 16 in [16]). The blisters [42] disappeared after keeping the samples in vacuum at 1 073 K (~ 15 min). By using Eq. (8), one can evaluate the quantity of $\tau_{0.63(des.)1073K[58]} \approx 5$ min, which coincides (within the errors) with the similar

quantity of $\tau_{0.63(des.)1073K[17]} \approx 7$ min evaluated for graphene/SiC samples [17] (Item 10, Table 3).

A nearly complete decoration of the grain boundary network [24–34] can be imagined in Fig. 15(b) in [16] (from [43]). Also, as is seen in Fig. 16 in [16] (from [43]), such decoration of the nano-regions (obviously, located at the grain boundaries [24–34]) has a blister-like cross-section of height of about 1.7 nm and width of 10 nm order.

According to the thermodynamic analysis presented in Item 11, Eq. (15), such blister-like decoration nano-regions (obviously, located at the grain boundaries [24–34]) may contain the intercalated gaseous molecular hydrogen at a high pressure.

10. Consideration and interpretation of the PES/ARPES data [43] on hydrogenation-dehydrogenation of graphene/SiC samples

In [43], atomic hydrogen exposures at a pressure of $P_H \approx 1 \cdot 10^{-4}$ Pa and temperature $T = 973$ K on a monolayer graphene grown on the SiC(0001) surface are shown, to result in hydrogen intercalation. The hydrogen intercalation induces a transformation of the monolayer graphene and the carbon buffer layer to bi-layer graphene without a buffer layer. The STM, LEED, and core-level photoelectron spectroscopy (PES) measurements reveal that hydrogen atoms can go underneath the graphene and the carbon buffer layer. This transforms the buffer layer into a second graphene layer. Hydrogen exposure (15 min) results initially in the formation of bi-layer graphene (blister-like) islands with a height of ~ 0.17 nm and a linear size of ~ 20–40 nm, covering about 40 % of the sample (Figs. 15(b), 15(e), 16(a) and 16(b) in [16] (from [43])). With larger (additional 15 min) atomic hydrogen exposures, the islands grow in size and merge until the surface is fully covered with bi-layer graphene (Figs. 15(c), 15(f), 16(c) and 16(d) in [16] (from [43])). A ($\sqrt{3} \times \sqrt{3}$) $R30º$ periodicity is observed on the bi-layer areas. Angle resolved photoelectron spectroscopy (ARPES) and energy filtered X-ray photoelectron emission microscopy (XPEEM) investigations of the electron band structure confirm that after hydrogenation the single π-band characteristic of monolayer graphene is replaced by two π-bands that represent bi-layer graphene. Annealing an intercalated sample, representing bi-layer graphene, to a temperature

of 1123 K or higher, re-establishes the monolayer graphene with a buffer layer on SiC(0001).

The dehydrogenation has been performed by subsequently annealing (for a few minutes) the hydrogenated samples at different temperatures, from 1023 to 1273 K. After each annealing step, the depletion of hydrogen has been probed by PES and ARPES (Figs. 17 and 18 in [16] (from [43])). From these data, by using Eqs. (8, 9), one can determine the following tentative quantities: $\tau_{0.63(des.)}$ (at 1023 K and 1123 K), $\Delta H_{(des.)} \approx 3.6$ eV and $K_{0(des.)} \approx 2 \cdot 10^{14}$ s^{-1} (Table 3).

The obtained value of the quantity of $\Delta H_{(des.)}$ coincides (within the errors) with values of the quantities of $Q_{app.IV} \approx 3.8$ eV $\approx \Delta H_{(C-H)"C","D"}$ (Item 4.2, Table 1B), which are related to the diffusion-rate-limiting TDS process IV [14] of a dissociative chemisorption of molecular hydrogen in defected regions in graphite materials (Table 1B), and to the chemisorption models "C" and "D" (Fig. 4 in [16]).

The obtained value of the quantity of $K_{0(des.)}$ may be correlated with possible values of the (C-H) bonds' vibration frequency ($\nu_{(C-H)"C","D"}$). Hence, by taking also into account that $\Delta H_{(des.)} \approx \Delta H_{(C-H)"C","D"}$, one may suppose the case of a non-diffusion-rate-controlling process corresponding to the Polanyi-Wigner model [14].

On the other hand, by taking also into account that $\Delta H_{(des.)} \approx \Delta H_{(C-H)"C","D"}$, one may suppose the case of a diffusion-rate-controlling process corresponding to the TDS process IV [14] (Table 1B). Hence, by using the value [14] of $D_{0app.IV} \approx 6 \cdot 10^2$ cm^2/s, one can evaluate the quantity of $L \approx (D_{0app.IV} / K_{0(des.)})^{1/2} = 17$ nm (Table 3). The obtained value of L (also, as and in the case of (SiC-D/QFMLG) [39], item 7, Table 2) coincides (within the errors) with values of the quantities of $L_{def.} \approx 11 - 17$ nm (Item 5, Eq. (10)) and $L_{def.} \approx 20$ nm (Item 6, Fig. 8(b) in [16] (from [37, 38])). The obtained value of L is also correlated with the STM data (Figs. 15 and 16 in [16] (from [43])). It shows that the desorption process of the intercalated hydrogen may be rate-limited by diffusion of hydrogen atoms to a nearest one of the permeable defects of the anchored graphene layer.

When interpretation of these results, one can also take into account the model (proposed in [43]) of the interaction of hydrogen and silicon atoms at the graphene-SiC interface resulted in Si-C bonds at the intercalated islands.

11. Consideration and interpretation of the TDS/STM data [44, 45] for HOPG treated by atomic hydrogen

In [44], atomic hydrogen accumulation in HOPG (high oriented pyrolytical graphite) samples and etching their surface under hydrogen thermal desorption (TD) have been studied by using a scanning tunneling microscope (STM) and atomic force microscope (AFM). STM investigations revealed that the surface morphology of untreated reference HOPG samples was found to be atomically flat (Fig. 19 (a) in [16]), with a typical periodic structure of graphite (Fig. 19 (b) in [16]). Atomic hydrogen exposure (treatment) of the reference HOPG samples (30–125 min at atomic hydrogen pressure $P_H \approx 10^{-4}$ Pa and a near-room temperature (~300 K)) with different atomic hydrogen doses (D), has drastically changed the initially flat HOPG surface into a rough surface, covered with nanoblisters with an average radius of ~25 nm and an average height of ~4 nm (Figs. 19 (c) and 19 (d) in [16]).

Thermal desorption (TD) of hydrogen has been found in heating of the HOPG samples under mass spectrometer control. As shown in Fig. 20 (a) in [16], with the increase of the total hydrogen doses (D) to which HOPG samples have been exposed, the desorbed hydrogen amounts (Q) increase and the percentage of D retained in samples approaches towards a saturation stage.

After TD, no nanoblisters were visible on the HOPG surface, the graphite surface was atomically flat, and covered with some etch-pits of nearly circular shapes, one or two layers thick (Fig. 20 (b) in [16]). This implies that after release of the captured hydrogen gas, the blisters become empty of hydrogen, and the HOPG surface restores to a flat surface morphology under the action of corresponding forces.

According to the concept [44], nanoblisters found on the HOPG surface after atomic hydrogen exposure are simply monolayer graphite (graphene) blisters, containing hydrogen gas in molecular form (Fig. 21 in [16]). As suggested in [44], atomic hydrogen intercalates between layers in the graphite net through holes in graphene hexagons, because of the small diameter of atomic hydrogen, compared to the hole's size, and is then converted to a H_2 gas form which is captured inside the graphene blisters, due to the relatively large kinetic diameter of hydrogen molecules.

However, such interpretation is in contradiction with that noted in Item 1 (Introduction) results [8, 46], that it is almost impossible for a hydrogen atom to pass through the six-membered ring of graphene at room temperature.

It is reasonable to assume (as it's been done in some previous Items) that in HOPG [44] samples atomic hydrogen passes into the graphite near-surface closed nano-regions (the graphene nanoblisters) through defects (perhaps, mainly through triple junctions of the grain and/or subgrain boundary network [24–34]) in the surface graphene layer. It is also expedient to note that in Fig. 20(b) in [16], one can imagine some grain boundary network decorated by the etch-pits.

The average blister has a radius of ~25 nm and a height ~4 nm (Fig. 19 in [16]). Approximating the nanoblister to be a semi-ellipse form, results in the blister area $S_b \approx 2.0 \cdot 10^{-11}$ cm^2 and its volume $V_b \approx 8.4 \cdot 10^{-19}$ cm^3. The amount of retained hydrogen in this sample becomes $Q \approx 2.8 \cdot 10^{14}$ H$_2$/cm^2 and the number of hydrogen molecules captured inside the blister becomes $n \approx (Q\, S_b) \approx 5.5 \cdot 10^3$. Thus, within the ideal gas approximation, and accuracy of one order of the magnitude, the internal pressure of molecular hydrogen in a single nanoblister at near-room temperature ($T \approx 300$ K) becomes $P_{H_2} \approx \{k_B\, (Q\, S_b)\, T\, /\, V_b\} \approx 10^8$ Pa. The hydrogen molecular gas density in the blisters (at $T \approx 300$ K and $P_{H2} \approx 1 \cdot 10^8$ Pa) can be estimated as $\rho \approx \{(Q\ M_{H_2}\ S_b)/V_b\} \approx 0.045$ g/cm^3, where M_{H_2} is the hydrogen molecule mass. It agrees with data [47] considered in [16], on the hydrogen (protium) isotherm of 300 K.

These results can be **quantitatively** described, with an accuracy of one order of magnitude, with the thermodynamic approach [21], by using the condition of the thermo-elastic equilibrium for the reaction of (2H$_{(gas)}$ → H$_{2(gas\_in\_blisters)}$), as follows [15, 16]:

$$(P_{H_2} / P_{H_2}^0) \approx (P_H / P_H^0)^2 \exp\left\{\left[\square H_{dis} - T\square S_{dis} - P*_{H_2}\square V)\right]/k_B T\right\} \tag{11}$$

where $P*_{H_2}$ is related to the blister "wall" back pressure (caused by P_{H_2}) - the so called surface pressure [21] ($P*_{H_2} \approx P_{H_2} \approx 1 \cdot 10^8$ Pa), P_H is the atomic hydrogen pressure corresponding to the atomic flux [44] ($P_H \approx 1 \cdot 10^{-4}$ Pa), $P_{H_2}^0 = P_H^0 = 1$ Pa is the standard pressure [21], $\Delta H_{dis} = 4.6$ eV is the experimental value [22] of the dissociation energy (enthalpy) of one molecule of gaseous hydrogen (at room temperatures), $\Delta S_{dis} = 11.8\ k_B$ is the dissociation entropy [22], $\Delta V \approx (S_b\ r_b\ /\ n)$ is the apparent volume change, r_b is the radius of curvature of nanoblisters at the nanoblister edge ($r_b \approx 30$ nm, Figs. 19, 21(b) in [16]), N_A is the Avogadro number,

and T is the temperature ($T \approx 300$ K). The quantity of ($P^*_{H_2} \Delta V$) is related to the work of the nanoblister surface increasing with an intercalation of 1 molecule of H_2.

The value of the tensile stresses σ_b (caused by $P^*_{H_2}$) in the graphene nanoblister "walls" with a thickness of d_b and a radius of curvature r_b can be evaluated from another condition (equation) of the thermo-elastic equilibrium of the system in question, which is related to Eq. (11), as follows [15, 16]:

$$\sigma_b \approx (P^*_{H_2} \, r_b \, / \, 2d_b) \approx (\varepsilon_b E_b) , \tag{12}$$

where ε_b is a degree of elastic deformation of the graphene nanoblister walls, and E_b is the Young's modulus of the graphene nanoblister walls. Substituting in the first part of Eq. (12), the quantities of $P^*_{H_2} \approx 1 \cdot 10^8$ Pa, $r_b \approx 30$ nm and $d_b \approx 0.15$ nm results in the value of $\sigma_{b[15]} \approx 1 \cdot 10^{10}$ Pa.

The degree of elastic deformation of the graphene nanoblister walls, apparently reaches $\varepsilon_{b[15]} \approx 0.1$ (Fig. 21(b) in [16]). Hence, with Hooke's law of approximation, using the second part of Eq. (12), one can estimate, with the accuracy of one-two orders of the magnitude, the value of the Young's modulus of the graphene nanoblister walls: $E_b \approx (\sigma_b/\varepsilon_b) \approx 0.1$ TPa. It is close (within the errors) to the experimental value [48, 49] of the Young's modulus of a perfect (i.e. without defects) graphene ($E_{graphene} \approx 1.0$ TPa).

The experimental data [15, 59] on the thermal desorption (the flux J_{des}) of hydrogen from graphene nanoblisters in pyrolytic graphite can be approximated by three thermodesorption (TDS) peaks, i.e., # 1 with $T_{max\#1} \approx 1123$ K, # 2 with $T_{max\#2} \approx 1523$ K, and # 3 with $T_{max\#3} \approx 1273$ K. But their treatment, with using the above mentioned methods [14], is difficult due to some uncertainty relating to the zero level of the J_{des} quantity.

Nevertheless, TDS peak # 1 [59] can be characterized by the activation desorption energy $\Delta H_{(des.)1[59]} = 2.4 \pm 0.5$ eV, and by the per-exponential factor of the reaction rate constant of $K_{0(des.)1[59]} \approx 2 \cdot 10^{10}$ s^{-1} (Table 3). It points that TDS peak 1 [59] may be related to TDS peak (process) III in [14], for which the apparent diffusion activation energy is $Q_{app.III} = (2.6 \pm 0.3)$ eV and $D_{0app.III} \approx 3 \cdot 10^{-3}$ cm^2/s (Table 1B). Hence, one can obtain (with accuracy of one-two orders of the magnitude) a reasonable value of the diffusion characteristic size of $L_{TDS\text{-}peak1[59]} \approx$

$(D_{0app.III}/K_{0(des.)1[59]})^{1/2} \approx 4$ nm, which is obviously related to the separating distance between the graphene nanoblisters (Fig. 21(b) in [16]) or (within the errors) to the separation distance between etch-pits (Fig. 20(b) in [16]) in the HOPG specimens [15, 59].

As noted in Items 4.2 and 4.4, process III [14] is related to model "F*" (with $\Delta H_{(C-H)"F*"} = (2.5 \pm 0.3)$ eV), and it is a rate-limiting by diffusion of atomic hydrogen between graphene-like layers (in graphite materials and nanomaterials), where molecular hydrogen can not penetrate (according to analysis [14] of a number of the related experimental data).

Thus, TDS peak (process) 1 [15, 59] may be related to a rate-limiting diffusion of atomic hydrogen, between the surface graphene-like layer and neighboring (near-surface) one, from the graphene nanoblisters to the nearest penetrable defects of the separation distance $L_{TDS-peak1[59]} \sim 4$ nm.

12. Discussion

12.1. On some energetic characteristics of theoretical graphanes

In work [3], the stability of a diamond-like graphane CH (Fig. 1 in [16]) has been predicted on the basis of the first principles and total-energy calculations. This was concluded from the results of the calculations [3] of the two energetic characteristics: 1) binding energy $\Delta H_{bind.(graphane[3])}$ – the difference between the total energy of the isolated atoms and the total energy of the compounds; 2) the standard energy of formation $\Box H_{f\,298(graphane[3])}^{0}$ of the compounds ($CH_{(graphane[3])}$) from crystalline graphite ($C_{(graphite)}$) and gaseous molecular hydrogen ($H_{2(gas)}$) at the standard pressure and temperature conditions.

In the present study (Item 2), by using the $\Box H_{f\,298(graphane[3])}^{0}$ theoretical quantity and the thermodynamic method of cyclic processes [21], the following energetic characteristics (Table 1A) have been determined: 1) the break-down energy of C-H sp^3 bond in the graphane [3], relevant to the breaking away of one hydrogen atom from the material, $\Delta H_{(C-H)graphane[3]} = 2.5 \pm 0.1$ eV; 2) the break-down energy of C-C sp^3 bonds in the graphane [3], namely $\Delta H_{(C-C)graphane[3]?} \approx 4.9$ eV that is close to the similar quantity for graphene or graphite ($\Delta H_{(C-C)graphene[20]} = 4.93$ eV, $\Delta H_{(C-C)graphite[16,22]} = 4.94 \pm 0.03$ eV, Table 1A). On the other hand, by using the

$\Delta H_{bind.(graphane[3])}$ and $\Delta H_{(C-H)graphane[3]}$ quantities and the thermodynamic method of cyclic processes [21], the break-down energy of C-C sp^3 bonds in the graphane [3], namely $\Delta H_{(C-C)graphane[3]} \approx 2.7$ eV that is less than the similar quantity for diamond ($\Delta H_{(C-C)diamond[16,22]} = 3.69\pm 0.02$ eV, Table 1). This discrepancy between the $\Delta H_{(C-C)graphane[3]}$ and $\Delta H_{(C-C)graphane[3]?}$ values seems as an open question, relevance to some thermodynamic incompatibility of the $\Delta H^0_{f\,298(graphane[3])}$ and $\Delta H_{bind.(graphane[3])}$ theoretical values.

In work [20], the chemisorption of hydrogen on graphene was studied, using atomistic simulations, with a second generation reactive empirical bond order of Brenner inter-atomic potential. As it has been shown [20], the cohesive energy of graphane CH in the ground state is $\Delta H_{cohes.(graphane[20])} = 5.03$ eV/atom. This results in the binding energy of hydrogen, which is $\Delta H_{(C-H)graphane[20]} = 1.50$ eV/atom (Table 1A).

In the present study (Item 2), by using the $\Delta H_{cohes.(graphane[20])}$ and $\Delta H_{(C-H)graphane[20]}$, quantities and the thermodynamic method of cyclic processes [21], the break-down energy of C-C sp^3 bonds has been determined, namely $\Delta H_{(C-C)graphane[20]} = 2.35$ eV (Table 1A). On the other hand, by using the $\Delta H_{(C-H)graphane[20]}$ quantity only, i.e. without using the $\Delta H_{bind.(graphane[20])}$ quantity, one can evaluate, in the framework of the thermodynamic method of cyclic processes [21], a much higher value of the break-down energy of C-C sp^3 bonds in the theoretical graphane [20], namely $\Delta H_{(C-C)graphane[20]?} \approx 4.9$ eV that is close to the similar quantity for graphene or graphite ($\Delta H_{(C-C)graphene[17]} = 4.93$ eV, $\Delta H_{(C-C)graphite[16,22]} = 4.94 \pm 0.03$ eV, Table 1A). This large discrepancy between the $\Delta H_{(C-C)graphane[20]}$ and $\Delta H_{(C-C)graphane[20]?}$ values seems as an open question, as well, relevance to some thermodynamic incompatibility of the $\Delta H_{cohes.(graphane[20])}$ and $\Delta H_{(C-H)graphane[20]}$ theoretical values.

It is expedient also to point to a considerable discrepancy between the data [3] and data [20], relevance to values of some similar characteristics.

12.2. On dehydrogenation of theoretical graphane [4], comparing with the related experimental data [5]

In [4], the process of hydrogen thermal desorption from graphane [3] has been studied using the method of molecular dynamics.

In the present study (Item 3), the thermodynamic analysis of the theoretical data [4], by using the formal kinetics approximation and comparing with the experimental data [5] for a free-standing graphane membrane, has been done. It has been shown that the empirical [5] value of the relaxation time at 723 K ($\tau_{0.63(membr.[5])723K}$) is much larger (by about 3 orders), than the theoretical [4] one ($\tau_{0.63(graphane[4])723K}$), Table 1A. It is consistent with that mentioned in [5] suppositions that: (i) the experimental graphane membrane (a free-standing one) may have "a more complex hydrogen bonding, than the suggested by the theory"; (ii) graphane (CH) [3] may be "the until-now-theoretical material".

12.3. On the "thermodynamic forces" and/or energetics of forming (under atomic hydrogen treatment) of graphene nanoblisters in the surface HOPG layers and epitaxial graphenes

A number of researchers (for instance, [35–45]) has not considered (in a sufficient extent) the "thermodynamic forces" and/or energetics of forming (under atomic hydrogen treatment) of graphene nanoblisters in the surface HOPG layers and epitaxial graphenes.

Therefore, in this study (Items 3–11, Tables 1–3), the results of the thermodynamic analysis of the experimental (TDS, STM, STS, HREELS/LEED, PES, ARPS, Raman spectroscopy and others) data [5, 35–45] are presented. These results may be, particularly, used for interpretation of the data shown on Figs. 6–8, 11–16, 19–21 in [16]. The "thermodynamic forces" and/or energetics of forming (under atomic hydrogen treatment) of graphene nanoblisters in the surface HOPG layers and epitaxial graphenes have been considered and quantitatively described (Eqs. 11, 12). The physics of intercalation of molecular hydrogen nanophase of a high density into the graphene nanoblisters has been revealed. It is relevant for developing of a key breakthrough nanotechnology of the hydrogen on-board efficient and compact storage in fuel-cell-powered vehicles, i.e. for solving this very current, but long-term (from about 1995 year) problem.

12.4. On some nanodefects (grain boundaries, their triple junctions and others), penetrable for atomic hydrogen, in the surface HOPG layers and epitaxial graphenes

A number of researchers (for instance, [35–45]) has not taken into account (in a sufficient extent) the calculation results (for instance [8, 46]) showing that the barrier for the penetration of a hydrogen atom through the six-membered ring of a perfect graphene is larger than 2.0 eV. Thus, it is almost impossible for a hydrogen atom to pass through the six-membered ring of a perfect (i.e., without defects) graphene layer at room temperature.

Therefore, in this study, a real possibility of the atomic hydrogen penetration through some nanodefects in the graphene-layer-structures, i.e., grain boundaries, their triple junctions (nodes) and/or vacancies [24–34], is considered. These analytical results may be used for interpretation of the related data (for instance, Figs. 6–8, 11–16, 19–21 in [16]).

12.5. On finding and interpretation of the thermodynamic characteristics of "reversible" hydrogenation-dehydrogenation of epitaxial graphenes and membrane ones

A number of researchers (for instance, [3–5, 35–45]) has not treated and compared (in a sufficient extent) their data on "reversible" hydrogenation-dehydrogenation of membrane graphenes and epitaxial ones, with the aim of finding and interpretation of the thermodynamic characteristics.

Therefore, in this analytical study (Items 2–11, Tables 1–3), the thermodynamic approaches (particularly, Eqs. 1–12) have been used for treatment, some comparing, systematizing and interpretation of the theoretical and experimental data [3–5, 35–45].

As it is noted in 12.1, there is a considerable difference (out of the declared errors, and without any explanation) in theoretical values of the energetic graphane (CH) quantities ($\Delta H_{(C-H)}$, $\Delta H_{(bind.)}$, $\Delta H_{(C-C)}$) obtained in different theoretical studies, for instance, in [3] and [20] (Table 1A).

Unfortunately, the theoretical values of the graphane quantity of $\Delta H_{(C-C)}$ is not usually evaluated by the researchers and not compared by them with the much higher values of the graphene (both theoretical, and experimental) quantity of $\Delta H_{(C-C)}$ (Table 1A). It could be useful, for instance, when consideration of the fundamental strength properties of graphane and graphene structures.

12.6. On the thermodynamic characteristics and atomic mechanisms of "reversible" hydrogenation-dehydrogenation of free-standing graphene membranes

The thermodynamic analysis (Item 3) of experimental data [5] on "reversible" hydrogenation-dehydrogenation of free-standing graphene membranes has resulted in the following conclusive suppositions and/or statements.

1) These chemisorption processes are related to a non-diffusion-rate-limiting case. They can be described and interpreted within the physical model of the Polanyi-Wigner equation for the first order rate reactions [14–18], but not for the second order rate ones, as it is supposed, for instance, in [48].

2) The desorption activation energy is of $\Delta H_{des.(membr.[5])} = \Delta H_{C\text{-}H(membr.[5])} = 2.6 \pm 0.1$ eV (Table 1A). The value of the quantity of $\Delta H_{C\text{-}H(membr.[5])}$ coincides (within the errors), in accordance with the Polanyi-Wigner model [14–18], with the values of the similar quantities for theoretical graphanes [3, 4] (Table 1A) possessing of a diamond-like distortion of the graphene network. The value of the quantity of $\Delta H_{C\text{-}H(membr.[5])}$ coincides (within the errors) with the value of the similar quantity for model "F*" (Item 4.2, Table 1B) manifested in graphitic structures and nanostructures not possessing of a diamond-like distortion of the graphene network (an open theoretical question).

3) The desorption frequency factor is of $K_{0des.(membr.[5])} = \nu_{C\text{-}H(membr.[5])} \approx 5 \cdot 10^{13}$ s^{-1} (Table 1A); it is related to the corresponding vibration frequency for the C-H bonds (in accordance with the Polanyi-Wigner model for the first order rate reactions [14–18]).

4) The adsorption activation energy (in the approximation of $K_{0ads.} \approx K_{0des.}$) is of $\Delta H_{ads.(membr.[5])} = 1.0 \pm 0.2$ eV (Table 1A). The heat of adsorption of atomic hydrogen by the free standing graphene membranes [5] can be evaluated as [14, 21]: $(\Delta H_{ads.(membr.[5])} - \Delta H_{des.(membr.[5])}) = -1.5 \pm 0.2$ eV (an exothermic reaction).

5) Certainly, these tentative analytical results could be directly confirmed and/or modified by receiving and treating (within Eqs. (8, 9) approach) of the experimental data on $\tau_{0.63}$ at several annealing temperatures.

12.7. On the thermodynamic characteristics and atomic mechanisms of "reversible" hydrogenation-dehydrogenation of epitaxial graphenes

The thermodynamic analysis (Items 3–8, 10) of experimental data [5, 35–40, 43] on "reversible" hydrogenation-dehydrogenation of epitaxial graphenes has resulted in the following conclusive suppositions and/or statements.

1) These chemisorption processes for all 16 considered epitaxial graphenes [5, 35, 36, 39, 40, 43] (Tables 1A, 2, 3), unlike ones for the free-standing graphene membranes [4, 5] (Item 3, Table 1A), are related to a diffusion-rate-limiting case. They can be described and interpreted within the known diffusion approximation of the first order rate reactions [14–18], but not within the physical models of the Polanyi-Wigner equations for the first order rate reactions (as it is done, for instance, in [41, 42]) or for the second order rate reactions (as it is done, for instance, in [48]).

2) The averaged desorption activation energy for 14 of 16 considered epitaxial graphenes (Tables 1A, 2, 3) is of $\Delta H_{des.(epitax.)} = 0.5 \pm 0.4$ eV, and the averaged quantity of $\ln K_{0des.(epitax.)} = 5 \pm 8$, i.e., $K_{0des.(epitax.)} \approx 1.5 \cdot 10^2$ s^{-1} (or $5 \cdot 10^{-2}$ - $5 \cdot 10^5$ s^{-1}); the adsorption activation energy (in a rough approximation of $K_{0ads.} \approx K_{0des.}$) is of $\Delta H_{ads.(epitax.)} = 0.3 \pm 0.2$ eV.

3) The above obtained values of characteristics of dehydrogenation of the epitaxial graphenes can be presented, as follows: $\Delta H_{des.} \sim Q_{app.I}$, $K_{0des.} \sim (D_{0app.I} / L^2)$, where $Q_{app.I}$ and $D_{0app.I}$ are the characteristics of process I (Item 4.2, Table 1B), $L \sim d_{sample}$, i.e. being of the order of diameter (d_{sample}) of the epitaxial graphene samples. The diffusion-rate-limiting process I is related to the chemisorption models "F" and "G" (Fig. 4 in [16]). These results unambiguously point that in the epitaxial graphenes the dehydrogenation processes are rate-limiting by diffusion of hydrogen, mainly, from chemisorption "centers" (of "F" and/or "G" types (Fig. 4 in [16])) localized on the internal graphene surfaces to the frontier edges of the samples. These results point that the solution and the diffusion of molecular hydrogen may occur between the graphene layer and the substrate, unlike for a case of the graphene neighbor layers in graphitic structures and nanostructures, where the solution and the diffusion of only atomic hydrogen (but not molecular one) can occur (process III [14], Table 1B).

These results also allow to suppose that hydrogen atoms penetrate the graphene surface layer through some nanodefects (grain boundaries, their triple junctions and

others [24–34] penetrable for atomic hydrogen). Then, obviously, the hydrogen atoms associate to the molecular form, and

the formation of the graphene nanoblisters occurs, as it is discussed in point 12.3.

4) The above formulated interpretation (model) is direct opposite to the supposition (model) of a number of researchers, those believe in occurrence of hydrogen desorption (dehydrogenation) processes, mainly, from the external epitaxial graphene surfaces. And it is direct opposite to the supposition - model (noted in Item 1) of many scientists that the diffusion of hydrogen along the graphene-substrate interface is negligible.

5) In this connection, it is expedient to take into account also some other related experimental results, for instance [49–54], on the peculiarities of the hydrogenation-dehydrogenation processes in epitaxial graphenes, particularly, in the graphene-substrare interfaces.

Conclusion remarks

1. The thermodynamic analysis of the theoretical data [3, 20] for graphane, by using the thermodynamic method of cyclic processes [21], has shown that there is a thermodynamic incompatibility and discrepancy in values, relevance to some theoretical energetic characteristics (Table 1A); it is discussed in details in point 12.1.

2. The thermodynamic analysis of the theoretical data [4] on hydrogen thermal desorption from graphane, by using the formal kinetics approximation and comparing with the experimental data [5] for a free-standing graphane membrane, has shown that the empirical [5] value of the relaxation time at 723 K ($\tau_{0.63(membr.[5])723K}$) is much larger (by about 3 orders), than the theoretical [4] one ($\tau_{0.63(graphane[4])723K}$), Table 1A. It is consistent with the mentioned in [5] suppositions that: (i) the experimental graphane membrane (a free-standing one) may have "a more complex hydrogen bonding, than the suggested by the theory"; (ii) graphane (CH) [3] may be "the until-now-theoretical material".

3. The chemisorption processes in the free-standing graphene membranes are related to a non-diffusion-rate-limiting case. They can be described and interpreted

within the physical model of the Polanyi-Wigner equation for the first order rate reactions.

The desorption activation energy is of $\Delta H_{des.(membr.)} = \Delta H_{C\text{-}H(membr.)} = 2.6 \pm 0.1$ eV. It coincides, in accordance with the Polanyi-Wigner model, with the values of the similar quantities for theoretical graphanes (Table 1A) possessing of a diamond-like distortion of the graphene network. It also coincides (within the errors) with the value of the similar quantity (process III, model "F*" (Table 1B)) manifested in graphitic structures and nanostructures not possessing of a diamond-like distortion of the graphene network (an open theoretical question).

The desorption frequency factor is of $K_{0des.(membr.)} = \nu_{C\text{-}H(membr.)} \approx 5 \cdot 10^{13}$ s^{-1} (Table 1A). It is related, in accordance with the Polanyi-Wigner model, to the corresponding vibration frequency for the C-H bonds.

The adsorption activation energy (in the approximation of $K_{0ads.} \approx K_{0des.}$) is of $\Delta H_{ads.(membr.)} = 1.0 \pm 0.2$ eV (Table 1A). The heat of adsorption of atomic hydrogen by the free standing graphene membranes [5] may be as $(\Delta H_{ads.(membr.)} - \Delta H_{des.(membr.)}) = -1.5 \pm 0.2$ eV (an exothermic reaction).

4. The hydrogen chemisorption processes in epitaxial graphenes (Tables 1A, 2, 3), unlike ones for the free-standing graphene membranes (Table 1A), are related to a diffusion-rate-limiting case. They can be described and interpreted within the known diffusion approximation of the first order rate reactions, but not within the physical models of the Polanyi-Wigner equations for the first or for the second order rate reactions.

The desorption activation energy is of $\Delta H_{des.(epitax.)} = 0.5 \pm 0.4$ eV. The quantity of ln $K_{0des.(epitax.)}$ is of 5 ± 8, and the per-exponential factor of the desorption rate constant is of $K_{0des.(epitax.)} \approx 1.5 \cdot 10^2$ s^{-1} (or $5 \cdot 10^{-2}$ - $5 \cdot 10^5$ s^{-1}). The adsorption activation energy (in a rough approximation of $K_{0ads.} \approx K_{0des.}$) is of $\Delta H_{ads.(epitax.)} = 0.3 \pm 0.2$ eV.

The above obtained values of characteristics of dehydrogenation of the epitaxial graphenes can be presented as $\Delta H_{des.} \sim Q_{app.I}$ and $K_{0des.} \sim (D_{0app.I} / L^2)$, where $Q_{app.I}$ and $D_{0app.I}$ are the characteristics of process I (Table 1B), $L \sim d_{sample}$, i.e. being of the order of diameter (d_{sample}) of the epitaxial graphene samples. The diffusion-rate-limiting process I is related to the chemisorption models "F" and "G" (Fig. 4 in [16]). These results unambiguously point that in the epitaxial graphenes the

dehydrogenation processes are rate-limiting by diffusion of hydrogen, mainly, from chemisorption "centers" (of "F" and/or "G" types (Fig. 4 in [16])) localized on the internal graphene surfaces to the frontier edges of the samples. These results also point that the solution and the diffusion of molecular hydrogen occurs in the interfaces between the graphene layers and the substrates. It differs from the case of the graphene neighbor layers in graphitic structures and nanostructures, where only atomic hydrogen solution and diffusion can occur (process III, model "F*" [14], Table 1B).

These results also allow to suppose that hydrogen atoms penetrate the graphene surface layer through some nanodefects (grain boundaries, their triple junctions and others [24–34] penetrable for atomic hydrogen). Then, obviously, the hydrogen atoms associate to the molecular form, and the formation of the graphene nanoblisters occurs.

Such an interpretation (model) is direct opposite, relevance to the supposition (model) of a number of researchers, those believe in occurrence of hydrogen desorption processes, mainly, from the external epitaxial graphene surfaces. And it is direct opposite to the supposition-model of many scientists that the diffusion of hydrogen along the graphene-substrate interface is negligible.

5. The thermodynamic analysis of the experimental (TDS, STM, STS, HREELS/LEED, PES, ARPS, Raman spectroscopy and others) data [5, 35–45] have been done. The results may be, particularly, used for interpretation of the data shown on Figs. 6–8, 11–16, 19–21 in [16].

The "thermodynamic forces" and/or energetics of forming (under atomic hydrogen treatment) of graphene nanoblisters in the surface HOPG layers and epitaxial graphenes have been considered and quantitatively described (Eqs. 11, 12).

The physics of intercalation of molecular hydrogen nanophase of a high density into the graphene nanoblisters has been revealed. It is relevant for developing of a key breakthrough nanotechnology of the hydrogen on-board efficient and compact storage in fuel-cell-powered vehicles, i.e. for solving this very current, but long-term (from about 1995 year) problem. Some fundamental open questions on engineering of "super" hydrogen sorption in graphite nanofibers, relevance for clean energy applications are considered in [19].

Constructive critical discussions on the present and [14–19] results, and/or the International cooperation seem as a real way of a joint breakthrough solving of the hydrogen efficient storage problem.

There is some psychological barrier to be overcome, obviously existing for many scientists due to their numerous unsuccessful attempts in solving this problem.

Acknowledgments

References

1. Geim A. K., Novoselov K. S. The rise of graphene. *Nature Materials,* 2007, vol. 6, no. 3, pp. 183–191.

2. Palerno V., Not a molecule, not a polymer, not a substrate…the many faces of graphene as a chemical platform. *Chemical Communications*, 2013, vol. 49, no. 28, pp. 2848–2857.

3. Sofo J.O., Chaudhari A.S. and Barber G.D. Graphane: A two-dimensional hydrocarbon. *Phys. Rev. B*, 2007, vol. 75, pp. 153401–1–4.

4. Openov L.A., Podlivaev A.I. Thermal desorption of hydrogen from graphane. *Technical Physics Letters*, 2010, vol. 36, no. 1, pp. 31–33.

5. Elias D.C., Nair R.R., Mohiuddin T.M.G., Morozov S.V., Blake P., Halsall M.P., Ferrari A.C., Boukhvalov D.W., Katsnelson M.I., Geim A.K. and Novoselov K.S. Control of graphene's properties by reversible hydrogenation: evidence for graphane. *Science*, 2009, vol. 323 (5914), pp. 610–626.

6. Openov L.A., Podlivaev A.I. Thermal stability of single-side hydrogenated graphene. *Technical Physics*, 2012, vol. 57, no. 11, pp. 1603–1605.

7. Pujari B.S., Gusarov S., Brett M. and Kovalenko A. Single-side-hydrogenated graphene: Density functional theory predictions. *Physical Review B*, 2011, vol. 84, pp. 041402–1–6.

8. Xiang H.J., Kan E.J., Wei S.-H., Gong X.G. and Whangbo M.-H. Thermodynamically stable single-side hydrogenated graphene. *Physical Review B*, 2010, vol. 82, pp. 165425–1–4.

9. Podlivaev A.I., Openov L.A. On thermal stability of graphone. *Semiconductors*, 2011, vol. 45, no. 7, pp. 958–961.

10. Nikitin A., X. Li, Z. Zhang, H. Ogasawara, H. Dai and A. Nilsson. Hydrogen storage in carbon nanotubes through the formation of stable C-H bonds. *Nano Lett.,* 2008, vol. 8, no. 1, pp. 162–167.

11.   Han S.S., Jung H., Jung D.H., Choi S.-H. and Park N. Stability of hydrogenation states of graphene and conditions for hydrogen spillover. *Phys. Rev. B – Condens. Matter. Mater. Phys*., 2012, vol. 85, no. 15, article # 155408.

12. Bauschlicher C.W. (Jr.), C. R. So. High coverages of hydrogen on (10.0), (9.0) and (5.5) carbon nanotubes. *Nano Lett*., 2002, vol. 2, no. 4, pp. 337–341.

13. Pimenova S.M., Melkhanova S.V., Kolesov V.P. and Lobach A.S. The enthalpy of formation and C-H bond enthalpy hydrofullerene $C_{60}H_{36}$. *J. Phys. Chem. B*, 2002, vol. 106, no. 9, pp. 2127–2130.

14. Nechaev Yu.S. Carbon nanomaterials, relevance to the hydrogen storage problem. *J. Nano Res*., 2010, vol. 12, pp. 1–44.

15. Nechaev Yu.S. Solid hydrogen in multigraphane nanostructures. *Intern. Sc. J. for Fundamental and Aplied Physics*, 2012, no. 01, pp. 38–60.

16. Nechaev Yu.S., Veziroglu T.N. Thermodynamic aspects of the stability of the graphene/graphane/hydrogen systems, relevance to the hydrogen on-board storage problem. *Advances in Materials Physics and Chemistry*, 2013, vol. 3, pp. 255–280.

17. Nechaev Yu.S., Veziroglu T.N. On thermodynamic stability of hydrogenated graphene layers, relevance to the hydrogen on-board storage. *The Open Fuel Cells Journal*, 2013, vol. 6, pp. 21–39.

18.. Nechaev Yu.S, Filippova V.P. , Yürüm A., Yürüm Yu., Veziroglu T.N. The reversible hydrogenation-dehydrogenation of membrane and epitaxial graphenes. *The Journal of Chemical Engineering and Chemistry Research*, 2014, no. 11, (in press).

19. Nechaev Yu.S., Yürüm A., Tekin A., Yavuz N.K., Yürüm Yu., Veziroglu T.N. Fundamental Open Questions on Engineering of "Super" Hydrogen Sorption in Graphite Nanofibers: Relevance for Clean Energy Applications. *The American Journal of Analytical Chemistry*, 2014, no. 11, (in press).

20. Dzhurakhalov A.A., F. M. Peeters. Structure and energetics of hydrogen chemisorbed on a single graphene layer to produce graphane. *Carbon*, 2011, vol. 49, pp. 3258–3266.

21. Bazarov I.P. Thermodynamics. Moscow: Vysshaya Shkola Publ., 1976 [in Russ.].

22. Karapet'yants M.K., Karapet'yants M.L. Osnovnye Termodinamicheskie Konstanty Neorganicheskikh i Organicheskikh Veshchestv [Fundamental Thermodynamic Constants of Inorganic and Organic Substances]. *Khimiya*, Moscow, 1968 [in Russ.].

23. Xie L., Wang X., Lu J., Ni Z., Luo Z., Mao H., Wang R., Wang Y., Huang H., Qi D., Liu R., Yu T., Shen Z., Wu T., Peng H., Oezyilmaz B., Loh K., Wee A.T.S., Ariando S., Chen W. Room temperature ferromagnetism in partially hydrogenated epitaxial graphene. *Applied Physics Letters*, 2011, vol. 98, no. 19, article # 193113.

24. Brito W.H., Kagimura R., Miwa R.H. Hydrogenated grain boundaries in graphene. *Applied Physics Letters*, 2011, vol. 98, no. 21, article # 213107.

25. Zhang T., Li X., Gao H. Defects controlled wrinkling and topological design in graphene. *Journal of the Mechanics and Physics of Solids, Applied Physics Letters*, 2014, vol. 67, pp. 2–13.

26. Banhart F., Kotakoski J. and Krasheninnikov A.V. Structural defects in graphene (Review). *ACS Nano,* 2011,vol. 5, no. 1, pp. 26–41.

27. Yazyev O.V., Louie S.G. Topological defects in graphene: Dislocations and grain boundaries. *Physical Review B - Condensed Matter and Materials Physics*, 2010, vol. 81, no. 19, article # 195420.

28. Kim K., Lee Z., Regan W., Kisielowki C., Crommie M.F., Zettl A. Grain boundary mapping in polycrystalline graphene. *ACS Nano*, 2011, vol. 5, no. 3, pp. 2142–2146.

29. Koepke J.C., Wood J.D., Estrada D., Ong Z.-Y., He K.T., Pop E., Lyding J.W. Atomic-scale evidence for potential barriers and strong carrier scattering at graphene grain boundaries: A scanning tunneling microscopy study. *ACS Nano*, 2013, vol. 7, no. 1, pp. 75–86.

30. Zhang J., Zhao J. Structures and electronic properties of symmetric and nonsymmetric graphene grain boundaries. *Carbon*, 2013, vol. 55, pp. 151–159.

31. Yakobson B.I., Ding F. Observational geology of graphene, at the nanoscale (Review). *ACS Nano*, 2011, vol. 5, no. 3, pp. 1569–1574.

32. Cockayne E., Rutter G.M., Guisinger N. P., Crain J.N., First P.N., Stroscio J.A. Grain boundary loops in graphene. *Physical Review B - Condensed Matter and Materials Physics*, 2011, vol. 83, no. 19, article # 195425.

33. Zhang J., Zhao J., Lu J. Intrinsic strength and failure behaviours of graphene grain boundaries. *ACS Nano*, 2012, vol. 6, no. 3, pp. 2704–2711.

34. Eckmann A., Felten A., Mishchenko A., Britnell L., Krupke R., Novoselov K.S., Casiraghi C. Probing the nature of defects in graphene by Raman spectroscopy. *Nano Letters,* 2012, vol. 12, no. 8, pp. 3925–3930.

35. Wojtaszek M., Tombros N., Garreta A., Van Loosdrecht P.H.M., Van Wees B.J. A road to hydrogenating graphene by a reactive ion etching plasma. *J. Appl. Phys.*, 2011, vol. 110, no. 6, article # 063715.

36. Castellanos-Gomez A., Wojtaszek M., Arramel, Tombros N., Van Wees B.J. Reversible hydrogenation and bandgap opening of graphene and graphite surfaces probed by scanning tunneling spectroscopy. *Small*, 2012, vol. 8, no. 10, pp. 1607–1613.

37. Castellanos-Gomez A., Arramel, Wojtaszek M., Smit R.H.M., Tombros N., Agraït N., Van Wees B.J., Rubio-Bollinger G. Electronic inhomogeneities in graphene: the role of the substrate interaction and chemical doping. *Boletin Grupo Español Carbón*, 2012, vol. 25, pp. 18–22.

38. Castellanos-Gomez A., Smit R.H.M., Agraït N., Rubio-Bollinger G. Spatially resolved electronic inhomogeneities of graphene due to subsurface charges. *Carbon*, 2012, vol. 50, no. 3, pp. 932–938.

39. Bocquet F.C., Bissn R., Themlin J.-M., Layet J.-M., Angot T. Reversible hydrogenation of deuterium-intercalated quasi-free-standing graphene on SiC(0001). *Physical Review B - Condensed Matter and Materials Physicsol*, 2012, vol. 85, no. 20, article # 201401.

40. Luo Z., Yu T., Kim K.-J., Ni Z., You Y., Lim S., Shen Z., Wang S., Lin J. Thickness-dependent reversible hydrogenation of graphene layers. *ACS Nano*, 2009, vol. 3, no. 7, pp. 1781–1788.

41. Hornekaer L., Šljivančanin Z., Xu W., Otero R., Rauls E., Stensgaard I., Lægsgaard E., Hammer B., Besenbacher F. Metastable structures and recombination pathways for atomic hydrogen on the graphite (0001) surface. *Phys. Rev. Lett.*, 2006, vol. 96, article # 156104.

42. Balog R., Jørgensen B., Wells J., Lægsgaard E., Hofmann P., Besenbacher F., Hornekær L. Atomic hydrogen adsorbate structures on graphene. *J. Am. Chem. Soc.*, 2009, vol. 131, no. 25, pp. 8744–8745.

43. Watcharinyanon S., Virojanadara C., Osiecki J.R., Zakharov A.A., Yakimova R., Uhrberg R.I.G., Johansson L.I. Hydrogen intercalation of graphene grown on 6H-SiC(0001). *Surface Science*, 2011, vol. 605, no. 17–18, pp. 1662–1668.

44. Waqar Z. Hydrogen accumulation in graphite and etching of graphite on hydrogen desorption. *J. Mater. Sci.*, 2007, vol. 42, no. 4, pp. 1169–1176.

45. Waqar Z., Klusek Z., Denisov E., Kompaniets T., Makarenko I., Titkov A., Saleem A. Effect of atomic hydrogen sorption and desorption on topography and electronic properties of pyrolytic graphite. *Electrochemical Society Proceedings*, 2000, vol. 16, pp. 254–265.

46. Jiang D., Cooper V.R., Dai S. Porous graphene as the ultimate membrane for gas separation. *Nano Lett.*, 2009, vol. 9, pp. 4019–4024.

47. Trunin R.F., Urlin V.D., Medvedev A.B. Dynamic compression of hydrogen isotopes at megabar pressures. *Phys. Usp.*, 2010, vol. 53, pp. 605–622.

48. Zhao X., Outlaw R.A., Wang J.J., Zhu M.Y., Smith G.D., Holloway B.C. Thermal desorption of hydrogen from carbon nanosheets. *The Journal of Chemical Physics*, 2006, vol. 124, pp. 194704–1–6.

49. Stolyarova E., Stolyarov D., Bolotin K., Ryu S., Liu L., Rim K.T., Klima M., Hybrtsen M., Pogorelsky I., Pavlishin I., Kusche K., Hone J., Kim P., Stormer H.L.,

Yakimenko V., Flynn G. Observation of graphene bubbles and effective mass transport under graphene films. *Nano Lett.*, 2009, vol. 9, iss. 1, pp. 332–337.

50. Riedel C., Coletti C., Iwasaki T., Starke U. Hydrogen intercalation below epitaxial graphene on SiC(0001). *Materials Science Forum*, 2010, vols. 645–648, pp. 623–628.

51. Riedel C., Coletti C., Iwasaki T., Starke U. Hydrogen intercalation below epitaxial graphene on SiC(0001). *Materials Science Forum*, 2010, vols. 645–648, pp. 623–628.

52. Goler S., Coletti C., Piazza V., Pingue P., Colangelo F., Pallegrini V., Emtsev K.V., Forti S., Starke U., Beltram F., Heun S. Revealing the atomic structure of the buffer layer between SiC(0001) and epitaxial graphene. *Carbon*, 2013, vol. 51, iss. 1, pp. 249–254.

53. Jones J.D., Morris C.F., Verbeck G.F., Perez J.M. Oxidative pit formation in pristin, hydrogenated and dehydrogenated graphene. *Appl. Surface Science*, 2012, vol. 10, pp. 1–11.

54. Lee M.J., Choi J.S., Kim J.-S., Byun I.-S., Lee D.H., Ryu S., Lee C., Park B.H. Characteristics and effects of diffused water between graphene and a SiO_2 substrste. *Nano Res.*, 2012, vol. 5, iss. 10, pp. 710–717.

Abstract

Herein, our modified results of thermodynamic analysis of some theoretical and experimental data on "reversible" hydrogenation and dehydrogenation of some graphene-layer-nanostructures are presented.

In the framework of the formal kinetics approximation of the first order rate reaction, some thermodynamic quantities for the reaction of hydrogen sorption (the reaction rate constant, the reaction activation energy, the per-exponential factor of the reaction rate constant) have been determined.

Some models and characteristics of hydrogen chemisorption on graphite (on the basal and edge planes) have been used for interpretation of the obtained quantities, with the aim of revealing the atomic mechanisms of hydrogenation and dehydrogenation of different graphene-layer-systems. The cases of both a non-diffusion rate limiting kinetics, and a diffusion rate limiting kinetics are considered.

On the basis of using the obtained analytical results of an empirical character (an indirect experiment), the physics of intercalation of molecular hydrogen nanophase of a high density into carbon-based nanostructures is considered.

It is relevant for developing of a key breakthrough nanotechnology of the hydrogen on-board efficient and compact storage in fuel-cell-powered vehicles – the very current, but long-term (from about 1995 year) problem.

A constructive critical discussion on our results and/or International co-operation seems as a real way of a joint breakthrough solving of the hydrogen storage problem.

Keywords: epitaxial and membrane graphenes; other graphene-layer-systems; hydrogenation-dehydrogenation; thermodynamic characteristics; intercalated hydrogen nanophase of a high density, atomic mechanisms (physics); the hydrogen efficient storage problem.